Published in final edited form as:

Cell Rep. 2020 January 07; 30(1): 124–136.e4. doi:10.1016/j.celrep.2019.12.015.

Mycobacterium tuberculosis limits host glycolysis and IL-1β by restriction of PFK-m via microRNA-21

Emer E Hackett[1], **Hugo Charles-Messance**[1], **Seónadh M O'Leary**[2], **Laura E Gleeson**[2], **Natalia Muñoz-Wolf**[1], **Sarah Case**[1], **Anna Wedderburn**[1], **Daniel G Johnston**[1], **Michelle Williams**[3], **Alicia Smyth**[4], **Mireille Ouimet**[5], **Kathryn J Moore**[5], **Ed C Lavelle**[1], **Sinead C Corr**[3], **Stephen V Gordon**[4], **Joseph Keane**[2], **Frederick J Sheedy**[1,6]

[1]School of Biochemistry & Immunology, Trinity College, Dublin 2, Ireland [2]School of Medicine, Trinity College, Dublin 2, Ireland [3]School of Genetics & Microbiology, Trinity College, Dublin 2, Ireland [4]School of Veterinary Medicine, University College Dublin, Ireland [5]New York University, School of Medicine, New York, NY, USA

SUMMARY:

Increased glycolytic metabolism recently emerged as an essential process driving host defence against *Mycobacterium tuberculosis* (Mtb), but little is known about how this process is regulated during infection. Here, we observe repression of host glycolysis in Mtb-infected macrophages, which was dependent on sustained up-regulation of the anti-inflammatory microRNA-21 (miR-21) by proliferating mycobacteria. The dampening of glycolysis by miR-21 was mediated through targeting of phospho-fructo-kinase, muscle isoform (PFK-m) at the committed step of glycolysis, which facilitated bacterial growth by limiting pro-inflammatory mediators, chiefly IL-1β. Unlike other glycolytic genes, PFK-m expression and activity is repressed during Mtb infection through miR-21-mediated regulation, while other less active isoenzymes dominate. Notably, IFNγ, which drives Mtb host defence, inhibits miR-21 expression, forcing an isoenzyme switch in the PFK-complex, augmenting PFK-m expression and macrophage glycolysis. These findings place targeting of PFK-m by miR-21 as a key node controlling macrophage immunometabolic function.

INTRODUCTION

Reprogramming of cellular metabolism has emerged as a directive mechanism controlling responses in immune cells (Pearce and Pearce, 2013). In particular, macrophages display an increased reliance the glycolytic pathway during inflammatory activation (Jha et al., 2015;

[6]Lead Contact: Dr. Frederick J Sheedy, Telephone: +353-1-8961612, fsheedy@tcd.ie.

AUTHOR CONTRIBUTIONS:

EJH & HCM performed and analysed all experiments. SMOL, LEG, AS & SVG provided assistance with Mtb infections. NMW, DGJ, MW, SC, AW, ECL & SCC provided assistance with miR-21-deficient animals. MO & KJM performed experiments in Fig. 1K. JK conceived ideas and co-supervised the work. FJS performed experiments, performed analysis, supervised the work and wrote the paper.

DECLARATION OF INTERESTS

The authors declare no competing interests.

DATA AND CODE AVAILABILITY

This study did not generate any unique datasets or code

Rodriguez-Prados et al., 2010). This is linked to pro-inflammatory processes including cytokine production (Tannahill et al., 2013), antigen presentation (Everts et al., 2014) and containment of bacteria (Garaude et al., 2016). We recently demonstrated the importance of glycolysis in host defence against the intracellular pathogen, *Mycobacterium tuberculosis* (Mtb) (Gleeson et al., 2018; Gleeson et al., 2016), which has evolved to replicate within macrophages of the pulmonary compartment (Huang et al., 2018). Failure to contain mycobacteria results in the development of tuberculosis – both latent and active infections, which coupled with increasing drug resistance and ineffective vaccines, has caused a global health crisis (O'Garra et al., 2013). Exploiting metabolic reprogramming, through manipulation of nutrients or by repurposing of existing drugs, will impact the development of novel immunotherapies and improved vaccines.

While several studies have documented increased glycolysis in Mtb-infected macrophages (Braverman et al., 2016; Gleeson et al., 2016; Huang et al., 2018; Lachmandas et al., 2016a; Lachmandas et al., 2016b), alongside the reprogramming of other metabolic pathways including lipid metabolism (Knight et al., 2018; Ouimet et al., 2016; Russell et al., 2009), little is known about how these pathways are regulated during infection and whether they play a role in defective immunity leading to disease. Additionally, macrophage ontogeny is known to affect immunometabolic responses, although the mechanisms controlling this remain unclear (Gleeson et al., 2018; Huang et al., 2018). Non-coding RNAs, particularly microRNAs, are important regulators of macrophage activation and innate immunity (Graff et al., 2012). MicroRNA-21 (miR-21) is one of the most highly expressed miRNAs in myeloid cells and emerged as an anti-inflammatory miRNA (Sheedy, 2015). We previously demonstrated that miR-21 is induced by TLR4 signalling to promote IL-10 production by limiting PDCD4 protein (Sheedy et al., 2010) and other groups have implicated this in efferocytosis, alongside negative regulation of TNF via targeting PTEN protein (Das et al., 2014). Dendritic cell activation and subsequent T-cell function is also limited by miR-21, via targeting IL12p35 mRNA (Lu et al., 2011). Expression of miR-21 has been reported in various cellular models of mycobacterial infection (Kumar et al., 2012; Wu et al., 2012) and importantly, was associated with dormancy in *Mycobacterium leprae* lesions, through negative regulation of multiple pro-inflammatory processes (Liu et al., 2012). However, its role in cellular metabolic programming is not known.

Since Mtb infection is known to favour the development of anti-inflammatory macrophages and evades pro-inflammatory mechanisms (O'Garra et al., 2013), we hypothesised that it would also evade host immunometabolic responses. Interestingly, we observe that persistent Mtb infection of macrophages was associated with negative regulation of host glycolysis and this was dependent on the induction of miR-21. Our data indicate that Mtb replication in macrophages was driven by suppression of metabolic reprogramming and associated IL-1β production, through miR-21. Crucially, we found that the specific control of glycolysis in Mtb-infected cells occurred through repression of a novel miR-21 target, at the rate-limiting and committed step of glycolysis (Tanner et al., 2018) - the phospho-fructo-kinase muscle (PFK-m) isoform, whose expression is dynamically regulated during Mtb infection to evade inflammation and in macrophage activation by IFNγ, to drive pro-inflammatory responses. Collectively, these data suggest that Mtb alters macrophage immunometabolic programming via miR-21 to ensure survival and replication.

RESULTS

Mtb infection attenuates metabolic reprogramming and drives anti-inflammatory miR-21

To further explore the mechanisms underlying metabolic reprogramming during Mtb infection, we treated bone-marrow derived macrophages (BMDM) with equivalent amounts of heat-killed Mtb H37Ra (hk-Mtb) or viable bacillus. Interestingly, we observed that hk-Mtb caused sustained accumulation of extracellular lactate over 72h similar to LPS treatment, indicative of increased glycolysis, whereas the viable bacillus was unable to induce lactate production to the same extent (Fig. 1A). This was associated with reduced ability of viable Mtb to promote IL-1β production, despite triggering similar TNF production (Supp. Fig. 1A–B) and reduced induction of pro-glycolytic genes after 24h infection, including *Slc2a1* (which encodes the glucose transporter GLUT1), hexokinase-2 (*Hk2*, which encodes the primary step in glycolysis) and lactate dehydrogenase-A (*LdhA*), the final glycolytic step for lactate production (Fig. 1B). A similar trend was observed when BMDM were infected with virulent Mtb H37Rv, with reduced lactate accumulation observed in cells infected with equivalent amounts of attenuated H37Ra or virulent H37Rv Mtb strains (ranging from 2-5 bacteria/cell), relative to a top dose of inactivated forms of each strain (iMtb – hk-Mtb for H37Ra or γ–irradiated Mtb (γMtb) for H37Rv) (Fig. 1C). A similar trend was observed in human cells, when human monocyte-derived macrophages (hMDMs - Supp. Fig. 1C) were infected with equal amounts of viable Mtb H37Ra or hk-Mtb H37Ra (Fig 1D). To confirm that persistent infection with Mtb can attenuate macrophage metabolic reprogramming over time, we modelled the primary host cell for Mtb *ex vivo* (Huang et al., 2018). Human alveolar macrophages (hAM) were isolated from donor bronchoalveolar lavage and infected *in vitro* with virulent Mtb H37Rv or γMtb H37Rv, alongside LPS treatment. Again, treatment with the inactive form was superior at inducing *IL1B* mRNA, although both forms induced similar *TNF* mRNA, which decreases over time (Fig. 1E). As previously observed (Gleeson et al., 2018), γMtb promoted the induction *SLC2A1* and *HK2*, while live Mtb infection is a poor inducer of these (Fig. 1E). No induction of *LDHA* was observed in these cells. Our results are supported by a recent report examining macrophage bioenergetics and the accumulation of glycolytic intermediates after virulent Mtb infection (Cumming et al., 2018) and together demonstrate that infection with Mtb, which adapts and grows within macrophages over time, negatively regulates the induction of glycolysis in macrophages.

To promote its own survival within macrophages, Mtb is known to induce anti-inflammatory mediators including IL-10 (Flynn et al., 1995; Pitt et al., 2012), which has been linked to negative regulation of glycolysis (Ip et al., 2017). However, we did not observe enhanced IL-10 production in BMDM infected with live Mtb (H37Ra or H37Rv) relative to inactivated forms, despite reduced IL-1β (Supp. Fig. 1D–J). We next examined the expression of another anti-inflammatory mediator linked to IL-10 production, the microRNA miR-21 (Sheedy et al., 2010). Notably, we observed dose-dependent induction of the bioactive mature miR-21 in both BMDM and hMDMs treated with increasing hk-Mtb or viable Mtb (Fig. 1F–G), with viable Mtb inducing significantly more miR-21 than equivalent amounts of hk-Mtb (Fig. 1F–G). This is preceded by early induction of the primary miR-21 containing transcript, *pri-miR-21* (Fig. 1H – 3-24 h post-infection),

implying elevated transcriptional up-regulation by live Mtb infection. A similar trend was observed when BMDM were infected with virulent or attenuated Mtb strains (H37Ra or H37Rv), with viable forms of both similarly driving enhanced mature miR-21 levels relative to inactivated forms 72 h post-infection (Fig 1I), with similar kinetics of *pri-miR-21* and mature miR-21 appearance (Supp. Fig. 1K). A similar effect was observed in hAMs with early upregulation of *pri-miR-21* preceding accumulation of mature miR-21 (Fig. 1J). Furthermore, lung tissue from mice infected *in vivo* with Mtb (Erdman strain) shows up-regulation of *pri-miR-21* at 30 days post-infection, which is maintained up to 53 days post-infection (Fig. 1K), indicative of an important role for miR-21 during chronic Mtb infection.

miR-21 limits glycolysis during Mtb infection

To investigate whether miR-21 impacts macrophage metabolism during Mtb infection, we utilized a mouse model of macrophage miR-21-deficiency. We isolated BMDM from WT and miR-21 loxP-targeted mice (Johnston et al., 2017) and confirmed similar numbers of CD11b-F4/80 double-positive cells (Supp. Fig. 2A). In resting miR-21-deficient BMDMs, both primary and mature miR-21 were undetectable and LPS-induced up-regulation of both transcripts was impaired, while levels of neighbouring *Tmem49* gene were unaffected (Supp. Fig. 2B). Functionally, *MiR-21*$^{-/-}$ BMDM express higher levels of miR-21 targets, *Pdcd4* and *Pten* mRNA, before and after LPS treatment, and consistent with earlier work (Sheedy et al., 2010), show impaired IL-10 production during TLR4 signalling (Supp. Fig. 2B–C). Upon infection with a moderate MOI (5 bacteria/cell) of Mtb H37Ra, we found that the production of lactate over time was dramatically enhanced in *MiR-21*$^{-/-}$ BMDM (Fig. 2A), although uptake of bacteria at 3h was similar between the two genotypes (Supp. Fig. 2D–E). Reduced lactate production was also observed when *MiR-21*$^{-/-}$ BMDM were infected with virulent Mtb H37Rv (Fig. 2B), which was not linked to altered viability since similar amounts of cell death were observed across both genotypes, measured using secreted LDH assay (Supp. Fig 2F). To validate the impact of miR-21 on glycolysis, we ablated miR-21 expression using antisense oligonucleotides in hMDMs. Reduction of basal and induced miR-21 by anti-miR-21 transfection was confirmed by qPCR (Supp. Fig. 2G). Silencing of miR-21 in hMDM increased lactate accumulation over the course of Mtb H37Ra infection suggestive of increased glycolysis and was similarly augmented in response to treatment with LPS or γMtb (Fig. 2C). While infection with Mtb H37Ra drives the induction of pro-glycolytic genes (e.g., *Slc2a1, Hk2* and *LdhA*) in BMDM in a dose-dependent fashion to similar levels as LPS treatment, expression of these genes is enhanced in miR-21-deficient cells (Fig. 2D). Enhanced induction of *Slc2a1* and *LdhA* mRNA was also observed in miR-21-deficient BMDM after infection with Mtb H37Rv strain (Supp. Fig. 3A). These data suggest that miR-21 limits macrophage metabolic reprogramming during Mtb infection.

To confirm the role of miR-21 in regulating the macrophage bioenergetic response, we performed extracellular flux analysis in resting BMDMs and BMDM treated with γMtb, since viable infection was not compatible with the exposed Seahorse system. While resting WT and *MiR-21*$^{-/-}$ BMDM display similar levels of both extracellular acidification (indicative of glycolytic activity) and oxygen consumption (a readout of tricarboxylic acid cycle (TCA)-fuelled oxidative phosphorylation), challenge with γMtb resulted in greater

ECAR in *MiR-21*$^{-/-}$ BMDM (Fig. 2E). Although both ECAR and OCR are similar across uninfected WT and *MiR-21*$^{-/-}$ BMDMs basally, when treated with oligomycin to block oxidative phosphorylation and allow maximal glycolysis, miR-21-deficient macrophages demonstrate a higher glycolytic reserve (GR) than WT cells (Fig. 2F). Furthermore, although GR is normally decreased after challenge with γMtb as cells begin to adopt glycolysis basally, *MiR-21*$^{-/-}$ BMDM retain a higher capacity for glycolysis than WT counterparts (Fig. 2F, Supp. Fig. 3B–C). Uncoupling the mitochondrial membrane with FCCP allows maximal oxidative phosphorylation and calculation of spare respiratory capacity (SRC), which is not significantly altered across genotypes basally. SRC decreases with γMtb treatment and this is more pronounced in miR-21-deficient cells, consistent with a higher glycolytic potential (Supp. Fig. 3D–F). However, the basal ratio of glycolysis relative to oxygen consumption shows a more pronounced shift toward glycolysis in *MiR-21*$^{-/-}$ BMDM, particularly pronounced for Mtb treatment, compared to WT BMDM (Fig. 2G). The increased potential for glycolysis was confirmed in hMDM transfected with anti-miR-21, which showed enhanced GR, without affecting SRC (Fig. 2H).

Restraint of glycolysis through miR-21 permits Mtb growth in macrophages

We next investigated how negative regulation of glycolysis by miR-21 impacts macrophage anti-mycobacterial responses. We observed similar levels of bacterial uptake in WT and miR-21-deficient macrophages by microscopy (Supp. Fig. 2D–E) and by measuring mycobacterial colony forming units (CFU) at 3 h post-infection (Supp. Fig. 4A). However, at later time points we noted a marked difference in the macrophages ability to contain Mtb. Although WT BMDM initially contain Mtb H73Ra, bacterial growth ensues at later times. *MiR-21*$^{-/-}$ BMDM permitted significantly less Mtb growth, with similar CFU numbers as baseline (Fig. 2I). Similar containment of virulent Mtb was observed in *MiR-21*$^{-/-}$ BMDM when viability of Mtb H37Rv was measured using bacterial chromosome specific probes as readouts of bacterial replication (Fig. 2J). This method was validated by Mtb H37Ra experiments which revealed similar patterns as detected by CFU methods, undetectable in cells treated with hk-Mtb (Supp. Fig. 4B–C). The decreased intracellular mycobacterial growth observed by multiple methods suggested an increased capacity of *MiR-21*$^{-/-}$ BMDM to respond to Mtb. Conversely, *MiR-21*$^{-/-}$ BMDM displayed increased levels of pro-inflammatory mediators linked to bacterial containment, including *Nos2* mRNA, a consequent reduction in Mtb-induced *Arg1* and more reactive nitrogen and oxygen species (Fig. 2K). Similar effects were observed in miR-21-silenced hMDM, displaying improved containment of Mtb H37Ra up to 5 days post-infection (Supp. Fig. 4D). To ascertain if the increased ability of miR-21-deficient macrophages to contain Mtb is linked to elevated glycolysis, we poisoned glycolysis using an inhibitor of the first hexokinase-mediated step in glycolysis, 2-deoxyglucose (2DG, Supp. Fig. 4E). Inhibition of glycolysis enhanced bacterial growth in WT BMDM and abrogated the protective effect of miR-21-deficiency (Fig. 2L, Supp. Fig. 4F). Importantly, 2DG also blocked the production of nitrite species in both WT and miR-21-deficient macrophages in response to LPS and γMtb treatment (Fig. 2M), implying that the anti-microbial response in *MiR-21*$^{-/-}$ BMDM is driven by increased glycolytic flux, normally limited by miR-21 induction.

Control of IL-1β production by miR-21 regulates anti-Mtb responses

To further investigate inflammatory responses suppressed by miR-21 regulation of glycolysis, we measured the production of various cytokines. Although miR-21 promotes IL-10 production in TLR4 signalling (Sheedy et al., 2010) (Supp. Fig. 5A), no significant difference in Mtb-induced IL-10 was observed in WT and miR-21-deficient macrophages, and addition of IL-10 to *MiR-21*$^{-/-}$ BMDM did not restore mycobacterial growth to WT levels (Supp. Fig. 5B–C). Furthermore, although Mtb-induced TNF production was enhanced in Mtb H37Ra-infected *MiR-21*$^{-/-}$ BMDM (Supp. Fig. 5D–E), neutralizing this with a blocking antibody which augments bacterial growth in WT cells, did not restore growth to WT levels in *MiR-21*$^{-/-}$ BMDM or alter levels of lactate production (Supp. Fig. 5F–G). We thus turned our attention to IL-1β, a cytokine central in host defence to Mtb and sensitive to changes in metabolism (Gleeson et al., 2016; Mayer-Barber et al., 2014). Levels of extracellular IL-1β increase at later times post-infection with both Mtb H37Ra and H37Rv and we observed a marked enhancement of IL-1β production in response to Mtb infection in *MiR-21*$^{-/-}$ BMDM relative to WT (Fig. 3A), as well as in miR-21-silenced hMDM (Fig. 3B). Conversely, transfection of BMDM with a miR-21 mimic reduced IL-1β secretion after Mtb H37Ra infection (Fig. 3C), confirming the ability of miR-21 to modulate IL-1β responses. Notably, blocking IL-1β using a specific antibody which significantly increases mycobacterial growth in WT cells, also increased mycobacterial growth in *MiR-21*$^{-/-}$ BMDM, restoring growth to WT levels (Fig. 3D).

Since IL-1β production is subject to multiple levels of regulation, we thus monitored the induction of *Il1b* mRNA in Mtb-infected macrophages and found this was significantly augmented by miR-21 deletion, particularly at later times post-infection in H37Ra and H37Rv infected BMDM (Fig. 3E). This effect on *IL1B* mRNA is also observed in miR-21-silenced hMDM (Supp. Fig. 5H). Increased glycolysis in macrophages potentiates late *Il1b* transcription via HIF-1α (Palsson-McDermott et al., 2015; Tannahill et al., 2013) and therefore, we examined if increased flux through glycolysis was fuelling the increased pro-inflammatory response in miR-21-deficient macrophages. Blocking glycolysis with 2DG abolished the increased *Il1b* mRNA levels in miR-21-deficient BMDM after Mtb infection or LPS treatment (Fig. 3F), implicating general transcriptional induction of the *Il1b* gene as a key process regulated by miR-21. Similar results were obtained in miR-21-silenced hMDM when glycolysis is circumvented by an alternative method, replacing glucose with galactose (Gohil et al., 2010) (Fig. 3G) , similar to 2DG-treated *MiR-21*$^{-/-}$ BMDM (Supp. Fig. 5I). To confirm the *in vivo* impact of miR-21 on Mtb-induced inflammation, we monitored cytokine levels in the murine peritoneal cavity after local injection of hk-Mtb (Martin et al., 2009). A small but significant increase was observed in TNF levels in lavage fluid from *MiR-21*$^{-/-}$ mice, with a more pronounced effect observed on *in vivo* IL-1β production, and no impact on IL-10 (Fig. 3H). Thus production of IL-1β is a key process fuelled by glycolysis and targeted by miR-21 to impact on the macrophage ability to contain Mtb.

miR-21 targets the expression of the glycolytic enzyme PFK-m

To confirm that increased glycolysis is a cause and not a consequence of increased inflammatory activity in miR-21-deficient macrophages, we monitored the effect of IL-1β

targeting on lactate production and observe similar levels in all cultures (Supp. Fig. 6A). Curiously, when we measured extracellular glucose in culture media, which decreases after infection due to increased metabolic activity (Supp. Fig. 6B), we did not observe differences across genotypes, although *MiR-21*$^{-/-}$ BMDM have increased glycolytic rates and produce more lactate. This suggested that the expression, and therefore activity, of a key process within the glycolytic pathway is directly impacted by miR-21. Although we previously observed increased induction of pro-glycolytic genes *Slc2a1, Hk2* and *LdhA* in *MiR-21*$^{-/-}$ BMDM (Fig 2D), these genes do not contain predicted binding sites for miR-21. Their enhanced production is likely a consequence of increased glycolytic activity activating HIF-1α (Palsson-McDermott et al., 2015), since this is abolished by 2DG treatment (Supp. Fig. 6C).

We therefore performed *in silico* analysis of glycolytic genes and found an isoform of the committed step of glycolysis (Mor et al., 2011), phospho-fructo-kinase muscle (PFK-M) which contains a predicted miR-21-binding site in its long 3'-UTR, conserved across multiple species including human and mouse. Other PFK isoforms (PFK-L (liver) and PFK-P (platelet)) have shorter 3'-UTRs and lack this sequence (Fig. 4A). To confirm the potential for miR-21 to directly repress *PFK-M* expression, we cloned its 3'UTR into a luciferase reporter. Plasmid-based overexpression of miR-21 dose-dependently decreases expression of the human *PFK-M* 3'UTR-linked reporter by ~30% in both HEK293Ts and the macrophage cell line RAW267.4 (Fig. 4B), with similar results obtained by co-transfection of miR-21 mimics (Supp. Fig. 6D). This repression was lost when the predicted miR-21-site is mutated (Fig. 4B). Consistent with metabolic reprogramming after infection or LPS activation of BMDM, the expression of *Pfk-l* and *Pfk-p* isoforms was enhanced, with higher induced-*Pfk-l* levels in miR-21-deficient cells (Fig. 4C). *Pfk-m* however, displays a differential expression pattern and is not induced by Mtb infection in WT cells (Fig. 4C). However when miR-21 is absent, increased *Pfk-m* mRNA is observed after infection with both H37Ra and H37Rv Mtb strains (Fig. 4C–D), supporting the notion that induction of miR-21 limits the expression of this isoform, which biochemical and genetic studies have suggested possesses an increased affinity for its substrate fructose-6-phosphate (Dunaway et al., 1988; Garcia et al., 2009) and therefore supports increased glycolysis. Importantly, baseline levels of *Pfk-m* mRNA are higher in *MiR-21*$^{-/-}$ BMDM, a trend not observed for other PFK isoforms and conversely, basal levels of *Pfk-m* mRNA are reduced by overexpression of miR-21 in RAW267.4 (Fig. 4E), similarly to *Pdcd4* mRNA, supporting the notion that this isoform represents a *bona-fide* miR-21-target. We thus examined protein expression, which miRNAs preferentially regulate (Selbach et al., 2008) and found that miR-21 overexpression dose-dependently reduced basal PFK-m protein levels in RAW267.4 macrophages (Fig. 4F). Although PFK-m protein levels are not significantly altered by Mtb infection in WT BMDM, levels are dramatically increased in both uninfected and infected *MiR-21*$^{-/-}$ BMDM (Fig. 4F). To confirm the elevated expression relates to augmented enzyme activity, we performed *in vitro* PFK activity assays by providing an excess of fructose-6-phosphate to cell lysates and monitoring the production of linked NADH. Uninfected wild-type BMDM had modest PFK activity which is actually decreased by Mtb infection, supporting the notion that during infection this key enzyme complex is targeted for negative regulation (Fig. 4G). This effect of infection was not observed when the earlier hexokinase step in the glycolytic

pathway is measured (Fig. 4G). When miR-21 is absent, untreated macrophages have significantly higher PFK, but not hexokinase activity (Fig. 4G), which is resistant to Mtb-induced regulation. PFK activity is determined by multiple isoforms with tissue-specific expression (Dunaway et al., 1988), but which can also form functional hetero-tetramers. Each isoform, PFK-l (liver), PFK-p (platelet) and PFK-m (muscle), are expressed in macrophages. To confirm the differences observed in *MiR-21*$^{-/-}$ BMDM were specifically due to altered PFK-M expression, we measured PFK activity in murine tissues with defined and restricted expression of each isoform. Specifically, we found that although liver tissue (which solely expresses PFK-L) from WT and *MiR-21*$^{-/-}$ mice displayed similar levels of PFK activity, cardiac muscle tissue (which solely expresses PFK-m) had significantly more PFK activity in *MiR-21*$^{-/-}$ mice (Fig. 4H), confirming that restriction of PFK-m by miR-21 controls metabolic activity *in vivo*. As before, no differences between genotypes was observed for hexokinase activity when measured *ex vivo* (Fig 4I). Thus, the increased PFK-1 activity measured in miR-21-deficient BMDM is likely due to altered expression of the PFK-m isoform. Lung tissue, the primary site of Mtb infection, expresses all 3 PFK isoforms (Shi et al., 2015). Despite this, a modest but significant increase in PFK enzyme activity is measured in lungs from *MiR-21*$^{-/-}$ animals (Fig. 4J), suggesting that miR-21 plays a role limiting glycolysis in this environment during the immune response.

Targeting of PFK-m by miR-21 controls Mtb responses

Since our results suggested an important role for PFK-m regulating glycolysis during Mtb infection which impacts on host defence, we more directly targeted *Pfk-m* itself, using siRNA. Although knockdown was not observed in uninfected BMDM, which express low basal levels of PFK-m protein, our siRNA transfection led to knockdown after treatment with hk-Mtb, which normally stabilises PFK-m protein expression and drives glycolysis (Fig. 5A). Importantly, the induction of glycolysis after hk-Mtb treatment was significantly impaired by PFK-m knockdown, as was the production of IL-1β (Supp. Fig 6A–B). During infection of BMDM with live Mtb H37Ra, we measured knockdown using qPCR and found significant reduction in basal *Pfk-m* mRNA levels (upto 50%, Fig. 5B), an effect mirrored by infection with Mtb H37Ra. Importantly, whereas the decrease in *Pfk-m* mRNA by Mtb infection is normally impaired in *MiR-21*$^{-/-}$ BMDM, siRNA transfection maintained this at low levels (Fig. 5B), allowing us to specifically examine the role of *Pfk-m* targeting my miR-21. The enhanced ability of *MiR-21*$^{-/-}$ BMDM to contain Mtb intracellular growth is lost when increased PFK-m expression is targeted by siRNA (Fig. 5C), confirming the importance if this molecule controlling the immunometabolic response to Mtb.

To confirm directly that this repression impacts Mtb responses, we employed a target protection strategy (Choi et al., 2007) to specifically block the interaction of *Pfk-m* mRNA and miR-21 (Fig. 5D). Transfection of WT BMDM with this oligonucleotide increased PFK-m protein levels in both uninfected and Mtb-infected macrophages (Fig. 5D). Similarly, extracellular levels of lactate and IL-1β were enhanced (Fig. 5E–F), as was the ability to contain intracellular Mtb (Fig. 5G). Importantly, these effects are phenocopied by, but not enhanced by oligonucleotide treatment in *MiR-21*$^{-/-}$ BMDM. Target protection does not alter the changes observed in Mtb-induced TNF or IL-10 production across genotypes (Supp. Fig. 6C–D). Collectively, these data support the notion that Mtb targets this key step

in the glycolytic pathway to limit host responses via persistent up-regulation of miR-21, which inhibits the expression of the pro-glycolytic PFK-m isoenzyme and subsequent activation of host defence through IL-1β production.

miR-21 impacts alveolar macrophage immunometabolic responses to Mtb

After confirming the importance of the miR-21/PFK-m axis in the model mouse BMDM & human MDM system, which mimic macrophages recruited to sites of infection, we investigated the primary host cell for Mtb, the resident AM, which we & others recently described as having metabolic plasticity dependent on both ontogeny & local environmental signals (Gleeson et al., 2018; Huang et al., 2018). First, we compared basal levels of mature miR-21 in mouse AM (mAM) or in mature BMDM and found strikingly higher levels of miR-21 in mAMs (Fig. 6A), also seen in hAM versus hMDM (Supp. Fig. 7A). AMs possess distinct metabolic properties from BMDM and induce less glycolysis after infection, therefore we measured maximal glycolytic capacity and found that mAM from *MiR-21*$^{-/-}$ mice have an increased GR over WT counterparts, more akin to BMDM, with no effect on SRC (Fig. 6B). Stimulation with γMtb induced modest extracellular lactate accumulation, which is enhanced in the absence of miR-21 (Fig. 6C). Infection with live Mtb H37Ra did not lead to a similar boost in lactate production in WT mAM, consistent with high levels of miR-21 & low glycolytic potential. However, although low, lactate induction was significantly enhanced in *MiR-21*$^{-/-}$ AM (Fig. 6C), supporting the notion that the presence of miR-21 exerts a limiting effect on the glycolytic potential of these cells. Little to no significant induction of *Slc2a1, Hk2* or *LdhA* mRNAs was observed in WT mAM after infection with viable Mtb H37Ra (Fig. 6D), unlike that seen in BMDM (Fig. 2D). However, more *Slc2a1* and *Hk2* mRNA induction is observed in *MiR-21*$^{-/-}$ mAM (Fig. 6D). We observed a trend towards basally higher *Pfk-m* mRNA (P = 0.07) in *MiR-21*$^{-/-}$ mAM than in WT and while infection with Mtb H37Ra decreased *Pfk-m* mRNA levels in WT mAM, this was stabilized and actually increased in *MiR-21*$^{-/-}$ mAM (Fig. 6D). With respect to host responses, there is significantly more accumulation of IL-1β protein in supernatants from Mtb-infected *MiR-21*$^{-/-}$ AM (Fig. 6E). A similar enhancement of *IL1B* mRNA is seen in hAM transfected with miR-21 antisense prior to activation with LPS (Supp. Fig. 7B). These results highlight the importance of miR-21 expression regulating the metabolic plasticity and immune phenotype of resident macrophages, which is influenced by both ontogeny and the nature of activating stimuli encountered during infection.

Activation of macrophages by IFNγ targets glycolysis via miR-21

We wondered whether other signals involved in the immune response could impact on the immunometabolic pathway via miR-21. Increased glycolysis has emerged as a cardinal feature of “M1” macrophages which have been treated *in vitro* with a TLR ligand (LPS) and IFNγ (Jha et al., 2015). In fact, IFNγ treatment of LPS-activated BMDM specifically enhances rates of glycolysis (Fig. 7A) and lactate production in Mtb-infected BMDM (Fig. 7B) and hMDM (Supp. Fig. 7C). Increased glycolysis is required for the potentiation of TLR-related genes including *Il1b* by IFNγ, since growing hMDM in galactose-containing media reduces the boost in IL1β production by IFNγ (Fig. 7C). IFNγ also supports enhanced induction of glycolytic genes (*Slc2a1, Hk2* and *Ldha*, Fig. 7D) during Mtb infection. Interestingly, the boost in IL1β expression by IFNγ is not apparent in miR-21-

silenced MDM (Fig. 7C) or *MiR-21*$^{-/-}$ BMDM (Supp. Fig. 7D). Intriguingly, the IFNγ-mediated boost in lactate production in WT BMDM reaches similar levels to that seen in miR-21-deficient cells (Fig. 7B, Supp. Fig. 7C), suggesting that IFNγ overcomes miR-21 repression of glycolysis, to promote its pro-inflammatory and anti-microbial activities. We therefore examined miR-21 levels in IFNγ-treated cells. Although IFNγ alters transcription of target genes (Hu and Ivashkiv, 2009), we did not observe alterations in *pri-miR-21* transcript levels in IFNγ-primed BMDM after 24 h LPS treatment or infection with Mtb H37Ra (Fig. 7E). However a decrease was noted in the levels of the mature miR-21 species after IFNγ treatment (Fig. 7E). This data suggest that IFNγ targets miR-21 production to temper its anti-inflammatory effects and negative regulation of glycolysis. Accordingly, *Pfk-m* mRNA, which normally decreases after Mtb infection, is maintained by IFNγ (Fig. 7E), with an increase in PFK-m protein expression in IFNγ-primed BMDM (Fig. 7F). This corresponds with a ~20% increase in PFK activity in Mtb-infected cells following IFNγ-priming, not observed in *MiR-21*$^{-/-}$ BMDM or at the level of hexokinase activity (Fig. 7G), suggesting that IFNγ counteracts the inhibitory effects of Mtb by buffering the increase in miR-21. Since IFNγ plays an important role in TB host defence (Bogunovic et al., 2012), we wondered if its anti-microbial effects proceeded through the miR-21/glycolysis axis. Again IFNγ treatment, which improves the macrophages ability to contain Mtb, is phenocopied by *MiR-21*$^{-/-}$ BMDM (Fig. 7H). This anti-microbial effect of IFNγ requires glycolysis, since it is blocked in both WT and *MiR-21*$^{-/-}$ BMDM by 2DG, which permits mycobacterial growth despite the presence of IFNγ (Fig. 7H). This places miR-21 expression as an important molecular switch which balances the immunometabolic response of macrophages, targeted by both pathogen and host-encoded processes to shape immunity.

DISCUSSION

By examining how Mtb manipulates innate immunity, we have identified a central regulator of the macrophage immunometabolic response – control of PFK-m expression, activity and glycolysis by a microRNA, miR-21. Whereas miR-21 was previously shown to negatively regulate innate immunity through modulating both pro and anti-inflammatory cytokine production (Barnett et al., 2016; Chen et al., 2013; Das et al., 2014; Liu et al., 2012; Lu et al., 2011; Merline et al., 2011; Sheedy et al., 2010), the engagement of a novel mRNA target by miR-21 in the context of Mtb infection points toward the importance of the immunometabolic response in host defence and expands the identified targets for miR-21 that regulate innate immunity.

It is now apparent that the nutrients utilized by and the metabolic pathways engaged determine immune cell function, but these can be manipulated by environmental signals – both activating and inhibitory (Hobson-Gutierrez and Carmona-Fontaine, 2018). While activation of macrophages by microbial-sensing TLRs, particularly TLR4, is known to subvert TCA (Jha et al., 2015) and lead to increased reliance on glycolysis driven by HIF1α (Rodriguez-Prados et al., 2010; Tannahill et al., 2013), less is known about the molecular mechanisms regulating this over time and during infection. We recently described the switch to increased glycolysis, critical for the macrophage ability to contain Mtb, early in infection (Gleeson et al., 2016). Here, we demonstrate that this is temporally regulated during infection, with blunting of this process apparent in macrophages infected with proliferating

mycobacteria. Furthermore, we show that augmenting production of mature miR-21 levels is central to mediating this control, suggesting that during infection, Mtb manipulates an endogenous host mechanism for the resolution of inflammation (Das et al., 2014), to co-opt macrophage function and maintain an environment favourable to bacillary replication.

Central to this is the production of IL-1β, which we and others have recently shown is critical in macrophage containment of Mtb (Gleeson et al., 2016; Mayer-Barber et al., 2014). Though IL-1β production is controlled at multiple levels (Prochnicki and Latz, 2017), in recent years it has been appreciated that later potentiation of its transcription occurs through HIF1α (Tannahill et al., 2013) – driven by increased glycolysis (Palsson-McDermott et al., 2015). Our work with Mtb, which drives both transcriptional induction and inflammasome activation (Mishra et al., 2010), revealed that miR-21 impacts upon IL-1β transcription, a finding not previously observed but upheld following induction of *Il1b* by the TLR4 ligand LPS. Even though miR-21 has been linked to negative regulation of pro-inflammatory processes including TNF production (Das et al., 2014; Liu et al., 2012) and promotion of anti-inflammatory responses like IL-10 (Das et al., 2014; Merline et al., 2011; Sheedy et al., 2010), this data places IL-1β as a key cytokine sensitive to regulation by miR-21 and is consistent with recent data from studies of leprosy (Liu et al., 2012). Although it has been suggested that *Il1b* mRNA is a direct target for repression by miR-21 (Liu et al., 2012; Terao et al., 2011), our data demonstrates indirect transcriptional regulation through modulating macrophage metabolism. Recently, multi-drug resistant strains of Mtb were shown to limit IL-1β production through reduced metabolic reprogramming (Howard et al., 2018). Although we use both attenuated (H37Ra) and virulent (H37Rv) lab Mtb strains for functional studies, in both cases negative regulation of glycolysis and pro-inflammatory signalling by miR-21 was observed. It may be the case that more clinically relevant and drug-resistant strains, which differentially modulate cytokine production may in fact mediate these effects through miR-21 induction and this remains to be tested.

Our studies of miR-21 deficient cells revealed unregulated glycolysis, despite intact glucose-fueled TCA basally. When interrogated Mtb did reduce SRC, which is consistent with an increased reliance on glycolysis and findings that Mtb infection of macrophages blocks fatty-acid oxidation to mobilize intracellular lipids (Knight et al., 2018; Ouimet et al., 2016; Russell et al., 2009). Therefore it is clear that the reprogramming of central energy metabolism observed during Mtb infection is distinct from the traditional “Warburg effect” observed in LPS-stimulated macrophages or tumor cells (Koppenol et al., 2011), with increased glycolytic rates a key feature of infected macrophages. We show that this is limited over time by targeting the expression of a pro-glycolytic isoenzyme of the rate-limiting PFK-1 step of glycolysis (Dunaway et al., 1988; Garcia et al., 2009; Tanner et al., 2018), which restricts flux through the glycolytic pathway and subsequent lactate production. These results are supported by a recent publication which noted decreased glycolysis and lactate accumulation in Mtb infected macrophages and through metabolic flux analysis of glycolytic intermediates, pointed toward regulation at the level of phosphofructokinse (Cumming et al., 2018). Increased metabolism of glucose through glycolysis has been suggested to promote macrophage activation by providing a rapid source of ATP, as well as increasing levels of biosynthetic precursors required for inflammatory responses. Intermediates of nucleotides, amino acids and lipids accumulate by feeding

anabolic pathways from glycolysis, including the pentose-phosphate pathway (PPP). Crucially, the decision to commit to this pathway is regulated by PFK-1 activity and a decrease in pro-glycolytic PFK-1 by Mtb-induced miR-21, may in fact support an alternative fate for carbon intermediates feeding into the PPP. Our observation that glucose consumption in WT and miR-21-deficent macrophages after infection remains unaltered, despite their ability to produce increased levels of lactate and increased PFK-1 activity, suggest a complex reprogramming of kinetics and nutrient utilization which is central to host/pathogen interactions. Targeting glycolysis at PFK-1, could allow bacteria to bypass host pro-inflammatory events fuelled by increased glycolysis (Braverman and Stanley, 2017; Garaude et al., 2016; Gleeson et al., 2016; Palsson-McDermott et al., 2015), yet support immune-evasion associated with altering intracellular anabolic pathways such as the PPP (Ouimet et al., 2016), including fatty acid synthesis or nucleotide production required for bacterial replication.

PFK-1 activity is also modulated by the host cytokine, IFNγ, during Mtb infection. By relieving the repression of PFK-1, through specifically modulating mature miR-21, IFNγ can reprogramme cellular metabolism to support pro-inflammatory activities. Consistent with this, IFNγ-driven HIF1α and NO production have emerged as key processes sensitive to changes in glycolysis (Braverman et al., 2016; Braverman and Stanley, 2017), that miR-21 also impact. Reprogramming of macrophage protein production by mTOR has been shown to be critical in IFNγ signaling (Su et al., 2015) and is mediated in part through modulation of miRNA levels. The specific negative regulation of the mature miR-21 species by IFNγ implies post-transcriptional regulation, previously observed for miR-21 during TGF-β signalling mediated through SMAD proteins (Su et al., 2015), which are also targets in IFNγ signalling (Ghosh et al., 2001). This results in increased PFK-m expression and subsequent glycolytic flux in activated macrophages, facilitating pro-inflammatory signaling. Apart from increased glycolytic flux, how altered metabolic activities and intermediates downstream of increased PFK-1 activity contribute to the pro-inflammatory and anti-microbial effects of IFNγ remain unclear. Recent studies suggest the mobilization of lipids in Mtb-infected cells contribute to IFNγ's activities (Knight et al., 2018) and the targeting of miR-21 observed here, could contribute to this by driving flux through glycolysis to promote glyceraldehyde 3-phosphate production. Novel anti-mycobacterial strategies promoting IFNγ activities are being developed and our work suggests these may proceed through modulating miRNA expression. Since recent work suggests that the metabolic activities of resident cells contribute to pulmonary compartment susceptibility to TB (Gleeson et al., 2018; Huang et al., 2018), a better understanding of the signals and mechanisms which underline this immunometabolic response, like our identification of a novel mRNA target and cellular process engaged by miR-21, provide rationale for boosting defective immunity in chronic infection like tuberculosis, but also other pulmonary diseases and cancer, where control of metabolic flux can have diverse and specific effects (Hobson-Gutierrez and Carmona-Fontaine, 2018).

STAR METHODS:

LEAD CONTACT AND MATERIALS AVAILABILITY

Frederick J Sheedy (fsheedy@tcd.ie) is Lead Contact for this study. All unique reagents generated in this study (plasmids, olignucoleotides) are available from the Lead Contact without restriction.

EXPERIMENTAL MODELS AND SUBJECT DETAILS

Animals—miR-21-deficient mice were generated by Taconic using Cre-loxP technology to delete the miR-21 coding region downstream of *Tmem49*. Following successful deletion, mice were back-crossed further to obtain a full body *MiR-21*$^{-/-}$ line described by (Johnston et al., 2017). Uncrossed mice were used as *MiR-21*$^{+/+}$ controls (WT). Mice were bred and maintained under specific pathogen-free conditions. Mature (> 12 week) male and female mice were used for cell extractions (BMDM, AMs) and were age and sex-matched. Intra-peritoneal injection experiments were carried out on 12-week old male mice. Whole lung RNA from mice infected with Mtb H37 Rv (Erdman strain) was described in (Ouimet et al., 2016). All experiments were carried out under approval of the Health Products Regulatory Authority, Ireland and Trinity College Dublin Animal Research Ethics Committee.

Cell isolation and culture—BMDM were isolated as described in Weischenfeldt et al, 2008, and re-plated at day 7 post-differentiation at 1x10^6 cell/mL in DMEM supplemented with 10% FBS and 5% L929-conditioned medium for experiments. Murine AM were isolated by bronchoalveolar lavage with ice-cold PBS via intratracheal insertion of a 20G IV catheter post-sacrifice. Cells were centrifuged from lavage fluid and plated in DMEM supplemented with 10% FBS and antibiotics (100 U/mL penicillin and 100 μg/mL streptomycin (Pen-Strep), counted and plated on plastic at 1x10^6 cell/mL to allow adherence of macrophages. Non-adherent cells were washed away after 24 h. Human AM were retrieved at bronchoscopy after informed consent. Bronchoalveolar lavage fluid was filtered through a 100-μm nylon strainer (BD Bioscience) and centrifuged at 1,400 rpm for 10 minutes. Cells were resuspended at 5×10^5 cells/ml in RPMI-1640 culture media supplemented with human serum (Sigma), 50 μg/ml fungizone, and 50 μg/ml cefotaxime. Adherence purification of AM was performed; non-adherent cells were removed by washing after 24 hours and experiments performed within 48 hours. Cells were plated at 5x10^5/ml. Work was approved by the Research Ethics Committee of St. James's Hospital. To generate human MDM, mononuclear cells were isolated from peripheral blood buffy coats obtained from the Irish Blood Transfusion Services (Dublin, Ireland) using density gradient centrifugation with Lymphoprep (Stem Cell Technologies). Cells were cultured on plastic in RPMI-1640 media supplemented with 10% human AB serum (Sigma-Aldrich) at 2 x 10^6/ml. Non-adherent cells were removed by washing every 2-3 days incubated for a total of 7 days to allow differentiation to macrophages prior to performance of experiments. Supply of human blood products from IBTS was approved by clinical indemnity to FJS. HEK293T cells were a gift from Clíona O'Farrelly (Trinity College Dublin) and were maintained in DMEM containing 10% FBS and Pen-Strep. RAW267.4 cells were a gift from Luke O'Neill (Trinity College Dublin) and were maintained in RPMI containing 10% FBS and Pen-Strep

***Mycobacterium tuberculosis* infections—**Non-viable irradiated *Mycobacterium tuberculosis* (Mtb) strain H37Rv was obtained from the American Type Culture Collection (ATCC) (Manassas, VA) and prepared according to manufacturer's instructions. Mtb strains H37Ra and H37Rv were also obtained from ATCC and propagated in Middlebrook 7H9 medium to log phase. On the day of infection, bacteria in log-phase were pelleted by centrifugation and resuspended in DMEM. Bacterial pellets were de-clumped by passing through a syringe with an 25G needle several times. A single cell suspension was isolated by centrifuging the bacterial suspension at 800 rpm for 3 min. The supernatant of this spin was quantified by spectrophotometry (OD_{600nm}) and used to infect macrophages. Preliminary assessment of multiplicity of infection (MOI) was performed for each experiment and genotype to allow normalisation for phagocytosis by infecting sample wells with varying amounts of resuspended Mtb for 3 h. For this, extracellular bacteria were removed by washing, cells fixed in 2% paraformaldehyde for 10 min and stained with Auramine O (Becton Dickinson) for acid-fast bacteria and with Hoechst 33358 (10μg/ml; Sigma-Aldrich) for cell nuclei to allow determination of the number of bacilli per cell by observing slides under an inverted fluorescent microscope (Nikon TE 300). Macrophages were infected at an MOI of 5 bacilli per cell (unless otherwise stated) for 3 h, extracellular bacteria removed by collecting the supernatant which was then purified further by centrifugation at 13,000 rpm for 10 min to pellet extracellular bacteria. Bacteria-free media was returned to macrophages after washing in DMEM to remove extracellular bacteria. Baseline growth was assessed by lysing 3 h time-point in 0.1% Triton-X for 10 min. Serial dilutions were plated on 7H10 Middlebrook Agar in triplicate and colony-forming units enumerated after incubation at 37°C for 14 – 21 days after plating. For later growth measurements this lysate was combined with pelleted extracellular bacteria, obtained by centrifugation of supernatant. For experiments with viable Mtb, macrophage supernatants were sterilised through 20 nM filters before use. For intra-peritoneal injection of heat-killed Mtb (hk-Mtb), 12-week mice were injected with 750 μg hk-Mtb (InVivoGen) in 1 mL in endotoxin-free 1x PBS. 24 h post-injection mice were sacrificed and the peritoneal cavity flushed out with 2 mL PBS. Lavage fluid was collected and concentrated (Amicon Ultra Ultracel 3K columns) for ELISA.

METHOD DETAILS

Gene Expression analysis—RNA was extracted with the RNeasy Kit (Qiagen), using a modified protocol to obtain small RNA species. For analysis of gene expression, cDNA was prepared with the High-Capacity cDNA Archive kit according to manufacturers' instructions (Applied Biosystems) and individual mRNAs were monitored with the following inventoried TaqMan assays (Applied Biosystems): mouse *18s* (Mm04277571_s1), human *18S* (Hs03003631_g1), mouse arginase-1 (*Arg-1*, Mm00475988_m1), mouse hexokinase-2 (*Slc2a1*, Mm00443385_m1), human hexokinase 2 (*SLC2A1*, Hs00606086_m1), mouse Hypoxanthine-guanine phosphoribosyltransferase (*Hprt*, Mm01545399_m1), human *HPRT* (Hs02800695_m1), mouse interleukin-1β (*Il1b*, Mm00434228_m1), human *IL1B* (Hs01555410_m1), mouse interleukin-10 (*Il10*, Mm00439614_m1), human *IL10* (Hs00961622_m1), mouse lactate dehydrogenase A (LdhA, Mm01612132_g1), human *LDHA* (Hs01378790_g1), mouse inducible nitric oxide synthase (*Nos2*, Mm00440502_m1), mouse programmed cell death 4 (*Pdcd4*, (Mm01266062_m1), human *PDCD4* (Hs00377253_m1), mouse phosphofructokinase isoform liver (*Pfk-l*, Mm00435587_m1),

human *PFKL* (Hs01036347_m1), mouse PFK isoform muscle (*Pfk-m*, Mm01309576_m1), human *PFKM* (Hs01075411_m1), mouse PFK isoform platelet (*Pfk-p*, Mm00444792_m1), human *PFKP* (Hs00737347_m1), mouse PTEN (Mm00477208_m1), human phosphatase and tensin homolog (*Pten*, Hs02621230_s1), mouse *Pri-miR-21* (Mm03306822_pri), human pri-miR-21 (Hs03302625_pri), mouse tumor necrosis factor-α (*Tnf*, Mm00443258_m1) and human *TNF* (Hs00174128_m1). The AB7900HT platform (Applied Biosystems) was used for all PCR, performed in triplicate in FAST mode. Changes in expression were calculated by the change in threshold (ΔΔCT) method with *Hprt* or 18S as an endogenous control and were normalized to results obtained in untreated cells. For miRNA analysis, individual miRNA TaqMan assays for the endogenous reference small RNA RNU6B and miR-21 were performed according to the manufacturer's instructions RNU6B (conserved) (001093) and miR-21 (conserved) (Hs04231424_s1) (Applied Biosystems). For measurement of mycobacterial viability by qPCR, RNA and genomic DNA was isolated simultaneously and measured using; Mtb IS6100 genomic DNA specific probe (custom designed probe) and Mtb 16s rRNA probes (Ba04230899_s1). For quantification, Mtb IS6100 expression in genomic DNA was normalized to bacterial housekeeping 16s rRNA and macrophage 18s rRNA expression in RNA samples and expressed relative to 3h post-infection using the ΔΔCT method.

Metabolic assays—Lactate concentration was measured in supernatants using the colorimetric Lactate Assay Kit (MAK064) (Sigma-Aldrich). Glucose concentration was measured using Glucose Assay Kit (ab65333) (Abcam). Enzyme activity was measured using kits from Sigma-Aldrich (Phosphofructokinase Activity Colorimetric Assay Kit MAK093 and Hexokinase Activity Colorimetric Assay Kit MAK091) according to manufacturer's instructions. Extracellular flux analyses were carried out using an XFe24 Extracellular Flux analyzer (Seahorse Biosciences) in Seahorse Media freshly supplemented with 10 mM glucose and 2 mM l-glutamine. Normalization for cell number was carried out with a Crystal Violet dye assay.

ELISA, Cell Viability, Nitrite and Intracellular ROS Assays—Cytokine concentration in supernatants were measured using sandwich ELISA READY-SET-GO kits from eBioscience according to the manufacturer's instructions. The following cytokines were assayed; mouse TNF (88-7324-77), mouse IL-10 (88-7105-77), mouse IL-1β (88-7013-77), human TNF (88-7346-77), human IL-10 (88-7106-77) and human IL-1β (88-7261-77. Cell viability was determined by measuring secreted lactate dehydrogenase using the CytoTox 96 Non-Radioactive Cytotoxicity Assay from Promega. Nitrite was measured in fresh supernatant using the Griess Reagent Nitrite Measurement Kit (Cell Signaling). Intracellular ROS were quantified using the DCFDA/H2DCFDA Cellular Reactive Oxygen Species Detection Assay Kit (ab113851) (Abcam).

Transfection and Plasmids—miR-21 specific miRNA inhibitors and mimics and non-targeting negative control molecules were obtained from Horizon Discovery/Dharmacon (miRIDIAN microRNA Hairpin Inhibitor Negative Control #1, miRIDIAN Hairpin Inhibitor hsa-miR-21-5p, miRIDIAN microRNA Mimic Negative Control #1 and miRIDIAN Hairpin Mimic hsa-miR-21-5p). Lipofectamine 2000 (Invitrogen) was used as a delivery agent.

$1x10^6$ MDM or BMDM were transfected 7 days after maturation with RNA:Lipofectamine complexes at concentration of 50 nM RNA molecule, 2 % Lipofectamine in serum-free OptiMEM media – left to complex at room temperature for 20 min prior to transfection. Cells were allowed to recover for 24 h before infection with Mtb. Luciferase activity was measured by transfecting HEK293T cells using GeneJuice (Merck) or RAW267.4 cells using Lipofectamine 2000 with a luciferase reporter plasmid miRNA 3'UTR target expression clone for Human PFKM (NM_000289.5) or a control mutated sequence (Genecopoeia) and assayed using the Dual-Luciferase kit (Promega). miR-21 was also overexpressed using pCMV-miR-21 or control vector pCMV-PL, both gifts from Bryan Cullen (Addgene plasmids 20381 & 20783). Target protection was achieved by transfecting cells using Lipofectamine 2000 to deliver the miR-21/PFK-M target protecting morpholino and control morpholino (5′-AGCTTATTTTTAGGAAAACTCTTGAGTAGC-3′) and 5′-ACCTTTTTTTTACGAAAACTGTTGAGTACC-3′) obtained from GeneTools (Oregon, USA). Mouse *Pfk-m* specific siRNA Horizon Discovery/Dharmacon (ON-TARGETplus Mouse *Pfk-m* (18642) siRNA) and BMDM were transfected using Lipofectamine 2000 to a top concentration of 50 nM and normalized with a non-targeting siRNA control 48h before further treatment/infection.

QUANTIFICATION AND STATISTICAL ANALYSIS

Statistical significance was assessed by one-way analysis of variance with multiple comparison tests using Prism 8 (Graph Pad software) or unpaired, two-tailed Student's t-test for single comparison using Microsoft Excel. P values of less than 0.05 were considered significant and denoted by * or #. Information on replicates/error/significance are indicated in the figure legends

Supplementary Material

Refer to Web version on PubMed Central for supplementary material.

ACKNOWLEDGEMENTS:

Support for this work came from Science Foundation Ireland Starting Investigator Grant (SFI/SIRG/2136) to FJS, (11/SIRG/B2099) to SCC and (15/IA/3154) to SVG, Health Research Board, Ireland (CSA/2012/16) and Royal City of Dublin Hospital Trust to JK and from the Irish Research Council (GOIPG/2017/1954) to SCC and (GOIPD/2019/807) to HCM.

REFERENCES

Barnett RE, Conklin DJ, Ryan L, Keskey RC, Ramjee V, Sepulveda EA, Srivastava S, Bhatnagar A, and Cheadle WG (2016). Anti-inflammatory effects of miR-21 in the macrophage response to peritonitis. J Leukoc Biol 99, 361–371. [PubMed: 26382295]

Bogunovic D, Byun M, Durfee LA, Abhyankar A, Sanal O, Mansouri D, Salem S, Radovanovic I, Grant AV, Adimi P, et al. (2012). Mycobacterial disease and impaired IFN-gamma immunity in humans with inherited ISG15 deficiency. Science 337, 1684–1688. [PubMed: 22859821]

Braverman J, Sogi KM, Benjamin D, Nomura DK, and Stanley SA (2016). HIF-1alpha Is an Essential Mediator of IFN-gamma-Dependent Immunity to Mycobacterium tuberculosis. J Immunol 197, 1287–1297. [PubMed: 27430718]

Braverman J, and Stanley SA (2017). Nitric Oxide Modulates Macrophage Responses to Mycobacterium tuberculosis Infection through Activation of HIF-1alpha and Repression of NF-kappaB. J Immunol 199, 1805–1816. [PubMed: 28754681]

Chen Y, Chen J, Wang H, Shi J, Wu K, Liu S, Liu Y, and Wu J (2013). HCV-induced miR-21 contributes to evasion of host immune system by targeting MyD88 and IRAK1. PLoS Pathog 9, e1003248. [PubMed: 23633945]

Choi WY, Giraldez AJ, and Schier AF (2007). Target protectors reveal dampening and balancing of Nodal agonist and antagonist by miR-430. Science 318, 271–274. [PubMed: 17761850]

Cumming BM, Addicott KW, Adamson JH, and Steyn AJ (2018). Mycobacterium tuberculosis induces decelerated bioenergetic metabolism in human macrophages. Elife 7.

Das A, Ganesh K, Khanna S, Sen CK, and Roy S (2014). Engulfment of apoptotic cells by macrophages: a role of microRNA-21 in the resolution of wound inflammation. J Immunol 192, 1120–1129. [PubMed: 24391209]

Dunaway GA, Kasten TP, Sebo T, and Trapp R (1988). Analysis of the phosphofructokinase subunits and isoenzymes in human tissues. Biochem J 251, 677–683. [PubMed: 2970843]

Everts B, Amiel E, Huang SC, Smith AM, Chang CH, Lam WY, Redmann V, Freitas TC, Blagih J, van der Windt GJ, et al. (2014). TLR-driven early glycolytic reprogramming via the kinases TBK1-IKKvarepsilon supports the anabolic demands of dendritic cell activation. Nat Immunol 15, 323–332. [PubMed: 24562310]

Flynn JL, Goldstein MM, Chan J, Triebold KJ, Pfeffer K, Lowenstein CJ, Schreiber R, Mak TW, and Bloom BR (1995). Tumor necrosis factor-alpha is required in the protective immune response against Mycobacterium tuberculosis in mice. Immunity 2, 561–572. [PubMed: 7540941]

Garaude J, Acin-Perez R, Martinez-Cano S, Enamorado M, Ugolini M, Nistal-Villan E, Hervas-Stubbs S, Pelegrin P, Sander LE, Enriquez JA, et al. (2016). Mitochondrial respiratory-chain adaptations in macrophages contribute to antibacterial host defense. Nat Immunol 17, 1037–1045. [PubMed: 27348412]

Garcia M, Pujol A, Ruzo A, Riu E, Ruberte J, Arbos A, Serafin A, Albella B, Feliu JE, and Bosch F (2009). Phosphofructo-1-kinase deficiency leads to a severe cardiac and hematological disorder in addition to skeletal muscle glycogenosis. PLoS Genet 5, e1000615. [PubMed: 19696889]

Ghosh AK, Yuan W, Mori Y, Chen S, and Varga J (2001). Antagonistic regulation of type I collagen gene expression by interferon-gamma and transforming growth factor-beta. Integration at the level of p300/CBP transcriptional coactivators. The Journal of biological chemistry 276, 11041–11048. [PubMed: 11134049]

Gleeson LE, Ryan D, O'Leary SM, McLaughlin AM, Sheedy FJ, and Keane JM (2018). Cigarette Smoking Impairs the Bioenergetic Immune Response to Mycobacterium Tuberculosis Infection. Am J Respir Cell Mol Biol.

Gleeson LE, Sheedy FJ, Palsson-McDermott EM, Triglia D, O'Leary SM, O'Sullivan MP, O'Neill LA, and Keane J (2016). Cutting Edge: Mycobacterium tuberculosis Induces Aerobic Glycolysis in Human Alveolar Macrophages That Is Required for Control of Intracellular Bacillary Replication. J Immunol 196, 2444–2449. [PubMed: 26873991]

Gohil VM, Sheth SA, Nilsson R, Wojtovich AP, Lee JH, Perocchi F, Chen W, Clish CB, Ayata C, Brookes PS, et al. (2010). Nutrient-sensitized screening for drugs that shift energy metabolism from mitochondrial respiration to glycolysis. Nat Biotechnol 28, 249–255. [PubMed: 20160716]

Graff JW, Dickson AM, Clay G, McCaffrey AP, and Wilson ME (2012). Identifying functional microRNAs in macrophages with polarized phenotypes. The Journal of biological chemistry 287, 21816–21825. [PubMed: 22549785]

Hobson-Gutierrez SA, and Carmona-Fontaine C (2018). The metabolic axis of macrophage and immune cell polarization. Dis Model Mech 11.

Howard NC, Marin ND, Ahmed M, Rosa BA, Martin J, Bambouskova M, Sergushichev A, Loginicheva E, Kurepina N, Rangel-Moreno J, et al. (2018). Mycobacterium tuberculosis carrying a rifampicin drug resistance mutation reprograms macrophage metabolism through cell wall lipid changes. Nat Microbiol 3, 1099–1108. [PubMed: 30224802]

Hu X, and Ivashkiv LB (2009). Cross-regulation of signaling pathways by interferon-gamma: implications for immune responses and autoimmune diseases. Immunity 31, 539–550. [PubMed: 19833085]

Huang L, Nazarova EV, Tan S, Liu Y, and Russell DG (2018). Growth of Mycobacterium tuberculosis in vivo segregates with host macrophage metabolism and ontogeny. J Exp Med 215, 1135–1152. [PubMed: 29500179]

Ip WKE, Hoshi N, Shouval DS, Snapper S, and Medzhitov R (2017). Anti-inflammatory effect of IL-10 mediated by metabolic reprogramming of macrophages. Science 356, 513–519. [PubMed: 28473584]

Jha AK, Huang SC, Sergushichev A, Lampropoulou V, Ivanova Y, Loginicheva E, Chmielewski K, Stewart KM, Ashall J, Everts B, et al. (2015). Network integration of parallel metabolic and transcriptional data reveals metabolic modules that regulate macrophage polarization. Immunity 42, 419–430. [PubMed: 25786174]

Johnston DGW, Kearney J, Zaslona Z, Williams MA, O'Neill LAJ, and Corr SC (2017). MicroRNA-21 Limits Uptake of Listeria monocytogenes by Macrophages to Reduce the Intracellular Niche and Control Infection. Front Cell Infect Microbiol 7, 201. [PubMed: 28589100]

Knight M, Braverman J, Asfaha K, Gronert K, and Stanley S (2018). Lipid droplet formation in Mycobacterium tuberculosis infected macrophages requires IFN-gamma/HIF-1alpha signaling and supports host defense. PLoS Pathog 14, e1006874. [PubMed: 29370315]

Koppenol WH, Bounds PL, and Dang CV (2011). Otto Warburg's contributions to current concepts of cancer metabolism. Nat Rev Cancer 11, 325–337. [PubMed: 21508971]

Kumar R, Halder P, Sahu SK, Kumar M, Kumari M, Jana K, Ghosh Z, Sharma P, Kundu M, and Basu J (2012). Identification of a novel role of ESAT-6-dependent miR-155 induction during infection of macrophages with Mycobacterium tuberculosis. Cell Microbiol 14, 1620–1631. [PubMed: 22712528]

Lachmandas E, Beigier-Bompadre M, Cheng SC, Kumar V, van Laarhoven A, Wang X, Ammerdorffer A, Boutens L, de Jong D, Kanneganti TD, et al. (2016a). Rewiring cellular metabolism via the AKT/mTOR pathway contributes to host defence against Mycobacterium tuberculosis in human and murine cells. Eur J Immunol 46, 2574–2586. [PubMed: 27624090]

Lachmandas E, Boutens L, Ratter JM, Hijmans A, Hooiveld GJ, Joosten LA, Rodenburg RJ, Fransen JA, Houtkooper RH, van Crevel R, et al. (2016b). Microbial stimulation of different Toll-like receptor signalling pathways induces diverse metabolic programmes in human monocytes. Nat Microbiol 2, 16246. [PubMed: 27991883]

Liu PT, Wheelwright M, Teles R, Komisopoulou E, Edfeldt K, Ferguson B, Mehta MD, Vazirnia A, Rea TH, Sarno EN, et al. (2012). MicroRNA-21 targets the vitamin D-dependent antimicrobial pathway in leprosy. Nature medicine 18, 267–273.

Lu TX, Hartner J, Lim EJ, Fabry V, Mingler MK, Cole ET, Orkin SH, Aronow BJ, and Rothenberg ME (2011). MicroRNA-21 limits in vivo immune response-mediated activation of the IL-12/IFN-gamma pathway, Th1 polarization, and the severity of delayed-type hypersensitivity. J Immunol 187, 3362–3373. [PubMed: 21849676]

Martin B, Hirota K, Cua DJ, Stockinger B, and Veldhoen M (2009). Interleukin-17-producing gammadelta T cells selectively expand in response to pathogen products and environmental signals. Immunity 31, 321–330. [PubMed: 19682928]

Mayer-Barber KD, Andrade BB, Oland SD, Amaral EP, Barber DL, Gonzales J, Derrick SC, Shi R, Kumar NP, Wei W, et al. (2014). Host-directed therapy of tuberculosis based on interleukin-1 and type I interferon crosstalk. Nature 511, 99–103. [PubMed: 24990750]

Merline R, Moreth K, Beckmann J, Nastase MV, Zeng-Brouwers J, Tralhao JG, Lemarchand P, Pfeilschifter J, Schaefer RM, Iozzo RV, et al. (2011). Signaling by the matrix proteoglycan decorin controls inflammation and cancer through PDCD4 and MicroRNA-21. Science signaling 4, ra75. [PubMed: 22087031]

Mishra BB, Moura-Alves P, Sonawane A, Hacohen N, Griffiths G, Moita LF, and Anes E (2010). Mycobacterium tuberculosis protein ESAT-6 is a potent activator of the NLRP3/ASC inflammasome. Cell Microbiol 12, 1046–1063. [PubMed: 20148899]

Mor I, Cheung EC, and Vousden KH (2011). Control of glycolysis through regulation of PFK1: old friends and recent additions. Cold Spring Harb Symp Quant Biol 76, 211–216. [PubMed: 22096029]

O'Garra A, Redford PS, McNab FW, Bloom CI, Wilkinson RJ, and Berry MP (2013). The immune response in tuberculosis. Annual review of immunology 31, 475–527.

Ouimet M, Koster S, Sakowski E, Ramkhelawon B, van Solingen C, Oldebeken S, Karunakaran D, Portal-Celhay C, Sheedy FJ, Ray TD, et al. (2016). Mycobacterium tuberculosis induces the miR-33 locus to reprogram autophagy and host lipid metabolism. Nat Immunol 17, 677–686. [PubMed: 27089382]

Palsson-McDermott EM, Curtis AM, Goel G, Lauterbach MA, Sheedy FJ, Gleeson LE, van den Bosch MW, Quinn SR, Domingo-Fernandez R, Johnston DG, et al. (2015). Pyruvate kinase M2 regulates Hif-1alpha activity and IL-1beta induction and is a critical determinant of the warburg effect in LPS-activated macrophages. Cell Metab 21, 65–80. [PubMed: 25565206]

Pearce EL, and Pearce EJ (2013). Metabolic pathways in immune cell activation and quiescence. Immunity 38, 633–643. [PubMed: 23601682]

Pitt JM, Stavropoulos E, Redford PS, Beebe AM, Bancroft GJ, Young DB, and O'Garra A (2012). Blockade of IL-10 signaling during bacillus Calmette-Guerin vaccination enhances and sustains Th1, Th17, and innate lymphoid IFN-gamma and IL-17 responses and increases protection to Mycobacterium tuberculosis infection. J Immunol 189, 4079–4087. [PubMed: 22972927]

Prochnicki T, and Latz E (2017). Inflammasomes on the Crossroads of Innate Immune Recognition and Metabolic Control. Cell Metab 26, 71–93. [PubMed: 28683296]

Rodriguez-Prados JC, Traves PG, Cuenca J, Rico D, Aragones J, Martin-Sanz P, Cascante M, and Bosca L (2010). Substrate fate in activated macrophages: a comparison between innate, classic, and alternative activation. J Immunol 185, 605–614. [PubMed: 20498354]

Russell DG, Cardona PJ, Kim MJ, Allain S, and Altare F (2009). Foamy macrophages and the progression of the human tuberculosis granuloma. Nat Immunol 10, 943–948. [PubMed: 19692995]

Selbach M, Schwanhausser B, Thierfelder N, Fang Z, Khanin R, and Rajewsky N (2008). Widespread changes in protein synthesis induced by microRNAs. Nature 455, 58–63. [PubMed: 18668040]

Sheedy FJ (2015). Turning 21: Induction of miR-21 as a Key Switch in the Inflammatory Response. Front Immunol 6, 19. [PubMed: 25688245]

Sheedy FJ, Palsson-McDermott E, Hennessy EJ, Martin C, O'Leary JJ, Ruan Q, Johnson DS, Chen Y, and O'Neill LA (2010). Negative regulation of TLR4 via targeting of the proinflammatory tumor suppressor PDCD4 by the microRNA miR-21. Nat Immunol 11, 141–147. [PubMed: 19946272]

Shi L, Salamon H, Eugenin EA, Pine R, Cooper A, and Gennaro ML (2015). Infection with Mycobacterium tuberculosis induces the Warburg effect in mouse lungs. Sci Rep 5, 18176. [PubMed: 26658723]

Su X, Yu Y, Zhong Y, Giannopoulou EG, Hu X, Liu H, Cross JR, Ratsch G, Rice CM, and Ivashkiv LB (2015). Interferon-gamma regulates cellular metabolism and mRNA translation to potentiate macrophage activation. Nat Immunol 16, 838–849. [PubMed: 26147685]

Tannahill GM, Curtis AM, Adamik J, Palsson-McDermott EM, McGettrick AF, Goel G, Frezza C, Bernard NJ, Kelly B, Foley NH, et al. (2013). Succinate is an inflammatory signal that induces IL-1beta through HIF-1alpha. Nature 496, 238–242. [PubMed: 23535595]

Tanner LB, Goglia AG, Wei MH, Sehgal T, Parsons LR, Park JO, White E, Toettcher JE, and Rabinowitz JD (2018). Four Key Steps Control Glycolytic Flux in Mammalian Cells. Cell Syst 7, 49–62 e48. [PubMed: 29960885]

Terao M, Fratelli M, Kurosaki M, Zanetti A, Guarnaccia V, Paroni G, Tsykin A, Lupi M, Gianni M, Goodall GJ, et al. (2011). Induction of miR-21 by retinoic acid in estrogen receptor-positive breast carcinoma cells: biological correlates and molecular targets. The Journal of biological chemistry 286, 4027–4042. [PubMed: 21131358]

Weischenfeldt J & Porse B Bone Marrow-Derived Macrophages (BMM): Isolation and Applications. CSH Protoc 2008, pdb prot5080 (2008).

Wu Z, Lu H, Sheng J, and Li L (2012). Inductive microRNA-21 impairs anti-mycobacterial responses by targeting IL-12 and Bcl-2. FEBS letters 586, 2459–2467. [PubMed: 22710123]

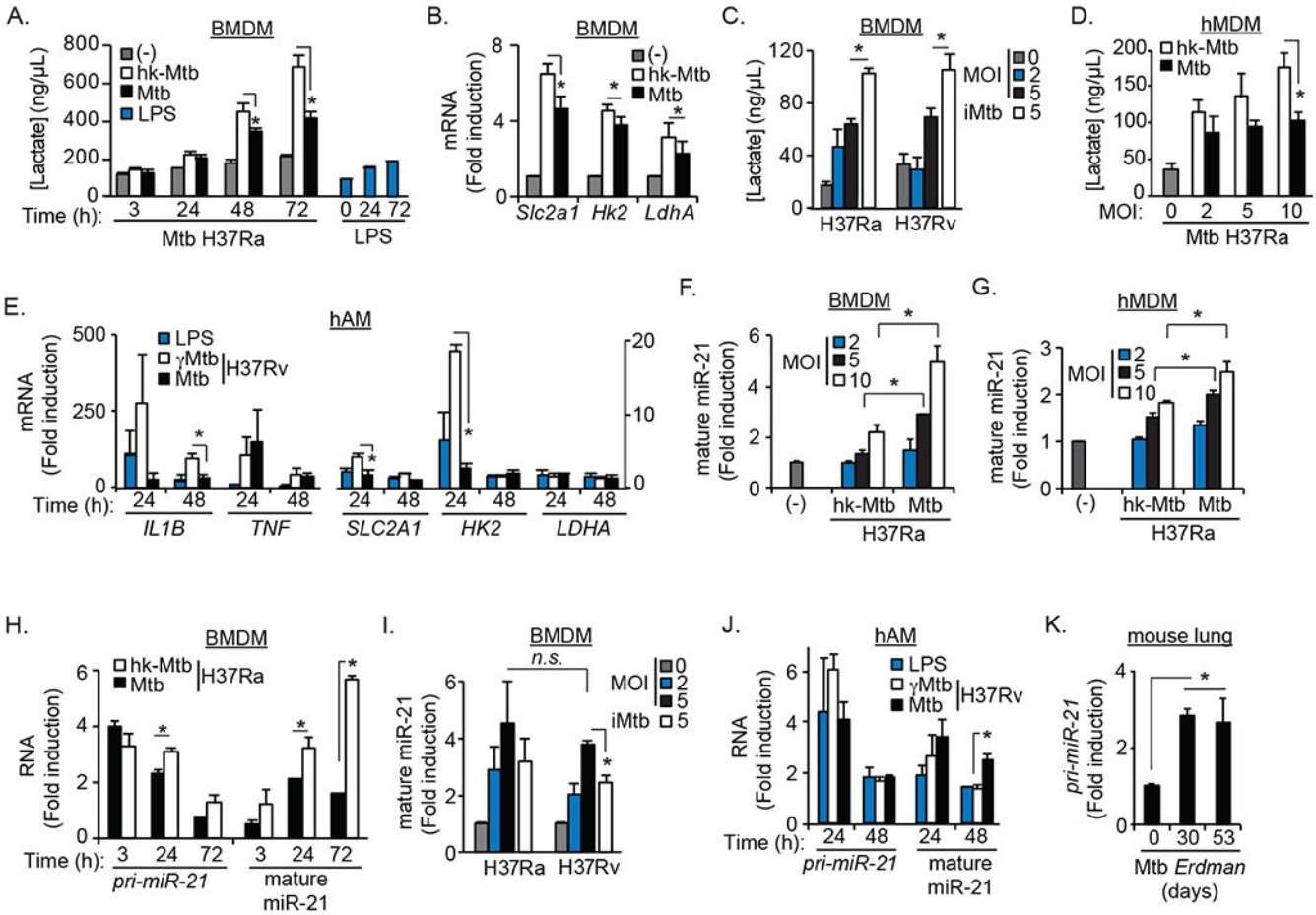

Figure 1.

Mtb infection attenuates macrophage metabolic reprogramming and drives miR-21. **A)** Extracellular lactate from bone-marrow derived macrophages (BMDM) infected with live *Mycobacterium tuberculosis* H37Ra (Mtb) or treated with heat-killed Mtb H37Ra (hk-Mtb) at a multiplicity of infection (MOI) of 5 bacteria/cell alongside LPS treatment (100 ng/mL) for indicated times. **B)** qPCR of indicated genes in BMDM treated as in A) for 24h. **C)** Extracellular lactate from BMDM infected with viable Mtb H37Ra or H37Rv strains at indicated MOI or treated with hk-Mtb H37Ra or γ-irradiated Mtb H37Rv (MOI 5) for 24h. **D)** Extracellular lactate from mature human monocyte-derived macrophages (hMDM) infected with Mtb as in A). **E)** qPCR analysis of the indicated genes in human alveolar macrophages (hAM) treated with viable Mtb H37Rv (Mtb) or γ-irradiated form (γMtb) at MOI of 2 or LPS (100 ng/mL) for 24-48 h. **F-H)** qPCR of mature miR-21 or primary miR-21 transcript (*pri-miR-21*) in BMDM (F,H) or hMDM (G) treated with hk-Mtb or infected with viable Mtb H37Ra (Mtb) at the indicated MOI for 24h (F-G) or at MOI of 5 for various times (0-72h – H). **I)** qPCR of mature miR-21 in BMDM treated as in C) for 72h. **J)** qPCR of the indicated RNA species in hAM treated as in E). **K)** qPCR of *pri-miR-21* expression in lung tissue from mice infected with Mtb (Erdmann strain) for the indicated time (days). Data is mean concentration ± sem for n=3 independent experiments (A,C-D,) mean fold-induction over uninfected cells ± sem for n=3 (B, G, I) or n=5 (F,H) independent

experiments, n=4 donors (E,J), or n=5 mice (K). * $P < 0.05$, n.s. $P > 0.05$ for the indicated group comparisons (ANOVA with post-hoc Tukey tests).

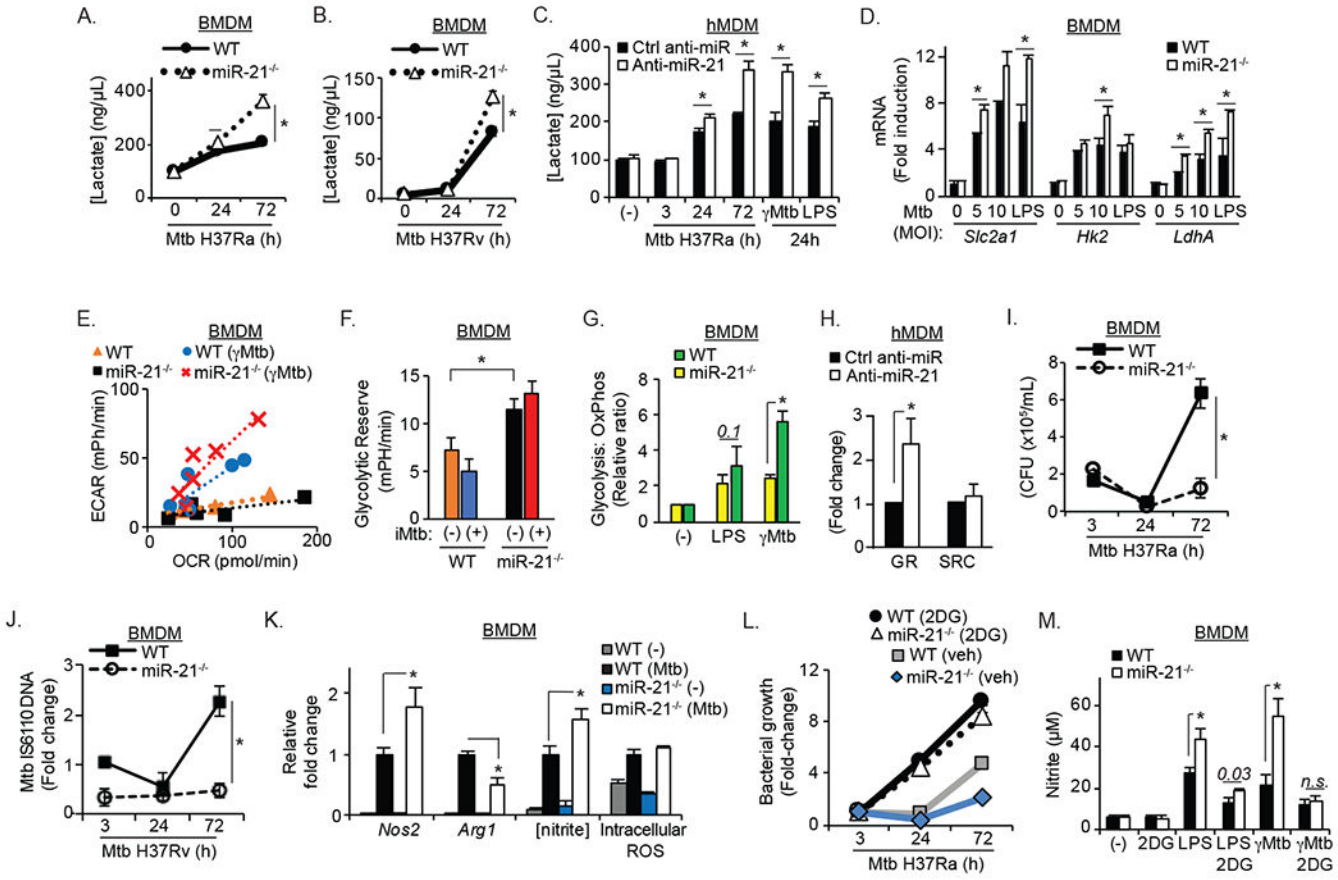

Figure 2.

Restraint of glycolysis by miR-21 permits Mtb growth in macrophages. **A-C)** Extracellular lactate from wild-type (WT) or miR-21-deficient (miR-21$^{-/-}$) BMDM infected with Mtb H37Ra (A) or Mtb H37Rv (B) (MOI 5) for indicated times or hMDM transfected with 50 nM miR-21-specific antisense (Anti-miR-21) or a control non-specific antisense (Anti-miR-Ctrl) prior to infection with Mtb H37Ra (MOI 5, indicated times) or treated with γMtb (MOI 5) or LPS (100 ng/mL) for 24 h (C). **D)** qPCR of indicated genes in BMDM infected with Mtb H37Ra at the indicated MOI or treated with LPS (100 ng/mL) for 24 h. **E)** Metabolic flux analysis of basal metabolism in untreated or γMtb-treated BMDM (indicated genotype, MOI 5, 24h) by measurement of extracellular acidification rate (ECAR) and oxygen consumption rate (OCR). **F)** Glycolytic Reserve (GR) of untreated or γMtb-treated BMDM (genotype indicated) treated with the indicated metabolic manipulations (Glu – addition of glucose, OM – oligomycin (1 μM), FCCP (1 μM) and Rotenone + antimycin A (0.5 μM)). **G)** ECAR:OCR ratio in BMDM treated with γMtb (MOI 5) or LPS (100 ng/mL) 24h. **H)** GR and Spare Respiratory Capacity (SRC) of resting hMDM transfected as in C) and treated with inhibitors as in G). **I)** Bacterial colony forming units (CFU) in BMDM infected with Mtb H37Ra (MOI 5) for the indicated times. **J)** qPCR of bacterial 1S6110 gDNA relative to 16s rRNA in BMDM infected with Mtb H37Rv (MOI 5) for the indicated times. **K)** Relative expression of indicated mediators in BMDM infected with Mtb H37Ra (Mtb, MOI 5, 24h). **L)** Bacterial CFU in BMDM treated with 2DG (10 mM) and

subsequently infected with Mtb H37Ra (MOI 5) as before. **M)** Nitrite species in supernatants from BMDM pre-treated with 2DG (10 mM) and subsequently treated with γMtb (MOI 5) or LPS (100 ng/mL) for 24 h. Data is mean concentration ± sem (A-C, M), mean fold-induction over uninfected cells ± sem (D,J), mean fold-change ± sem (F-H, K-L) or mean CFU ± sem (I) for n=3 independent experiments. Energy plot (E) presents mean values and H is mean ± sem from n=5 independent experiments. * $P < 0.05$, n.s. $P > 0.05$ for the indicated group comparisons (ANOVA with post-hoc Tukey tests or Student t-test (H).

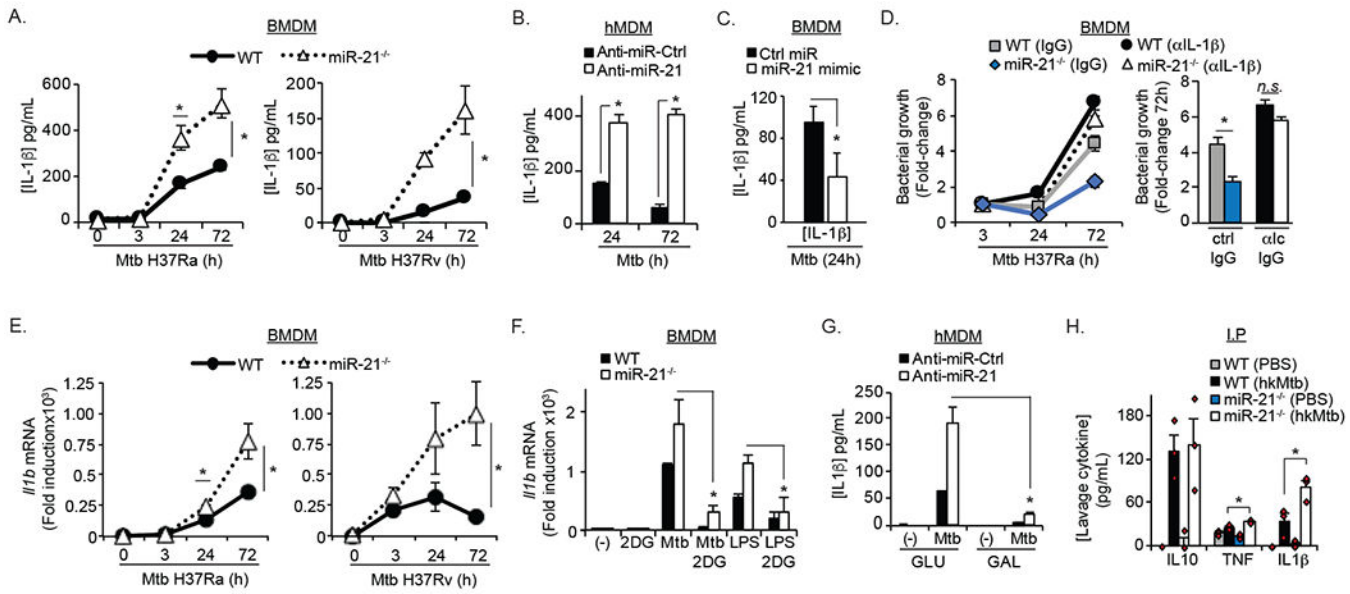

Figure 3.

Control of IL-1β production by miR-21 regulates anti-Mtb responses. **A-B)** IL-1β ELISA in supernatants from BMDM (genotype indicated) infected with Mtb H37Ra (A, left) or H37Rv (A, right) or hMDM transfected with 50 nM miR-21-specific antisense (Anti-miR-21) or a control non-specific antisense (Anti-miR-Ctrl) and subsequently infected with Mtb H37Ra (B) (MOI 5, indicated times. **C)** IL-1β ELISA in supernatants from BMDM transfected with 50 nM of miR-21-specific mimic (miR-21 mimic) or a control non-specific molecule (Ctrl-miR) infected with Mtb H37Ra (Mtb, MOI 5) for 24h. **D)** Bacterial growth in BMDM treated with anti-IL-1β specific antibody (αIL-1β, 1 μg/mL) or control IgG 3h post-infection with Mtb H37Ra as in A left). **E)** qPCR of *Il1b* mRNA in BMDM (genotype indicated) infected with Mtb H37Ra or H37Rv as before (A). **F)** qPCR of *Il1b* mRNA in BMDM pre-treated with 2DG (10 mM) infected with Mtb H37Ra (MOI 5) or treated with LPS (100 ng/mL) for 24 h. **G)** IL-1β ELISA in supernatants from hMDM transfected as in B), 24h prior to infection with Mtb H37Ra (MOI 5, 24h) in glucose-containing media (GLU) or glucose-free galactose-containing media (GAL). **H)** ELISA of indicated cytokines in lavage fluid taken from mice (genotype indicated) 24 h post-intraperitoneal injection of heat-killed Mtb (hk-Mtb, 750 μg per mouse) or PBS. Data (A-C, G-H) is mean concentration, fold-change in baseline CFU (3h) (D) and fold-induction over uninfected cells (E-F) and represents mean ± sem for n=4 (A, left panel) or n=3 (A right panel, B-G) independent experiments and for n=3 mice per group (H). * $P < 0.05$, n.s. $P > 0.05$ for the indicated group comparisons (ANOVA with post-hoc Tukey tests).

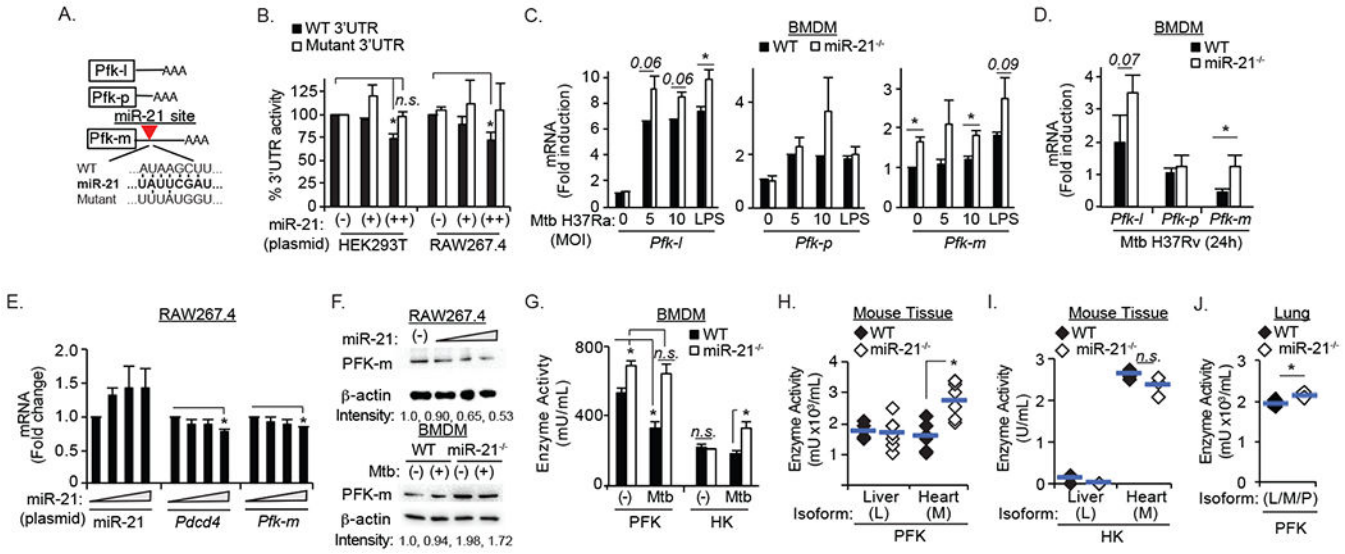

Figure 4.

miR-21 targets the expression of the glycolytic enzyme PFK-m. **A)** Schematic of PFK mRNAs indicating the miR-21 site & mutant constructs. **B)** 3'UTR luciferase reporter activity of PFK-m 3'UTR (WT 3'UTR) or mutant construct (Mutant 3'UTR) following co-transfection of HEK293T cells (left) or RAW267.4 cells (right) with control plasmid (−) or increasing amounts of miR-21 overexpressing plasmid (pCMV-miR-21, (+) 25ng per point, (++) 50ng per point). **C-D)** qPCR of PFK genes in BMDM infected with Mtb H37Ra at the indicated MOI or treated with LPS (100 ng/mL) for 24 h (C) or Mtb H37Rv (MOI 5, 24 h) (D). **E)** Relative expression of the indicated RNA species in RAW267.4 cells following 48 h transfection with increasing amounts of miR-21 overexpressing plasmid (pCMV-miR-21, 0-75ng per point). **F)** PFK-m immunoblot in RAW267.4 macrophages transfected with increasing amounts pCMV-miR-21 as in E (top panel) or BMDM (genotype indicated) before or after infection with Mtb H37Ra (MOI 5, 24h, bottom panel) alongside β-actin expression (loading control). **G)** In-vitro enzyme activity for phosphofructokinase (PFK) or hexokinase (HK) in BMDM lysates treated as in F. **H-J)** In-vitro PFK (H,J) or HK (I) enzyme activity in the indicated tissues from WT & miR-21$^{-/-}$ mice (20 mg tissue). Data is % inhibition relative to control transfected cells (A), fold-induction relative to uninfected or control transfected cells (C-E) or mean concentration with individual mouse values indicated (G-J). Blots are 1 experiment representative of n=3 independent experiments with normalized PFK-m band intensity provided underneath (F). Data is mean ± sem for n=5 (B-C, E, G) or n=3 (D) independent experiments or n=6 (J-I) or n=3 (J) mice per group (H-J). * $P < 0.05$, n.s. $P > 0.05$ for the indicated group comparisons (ANOVA with post-hoc Tukey tests).

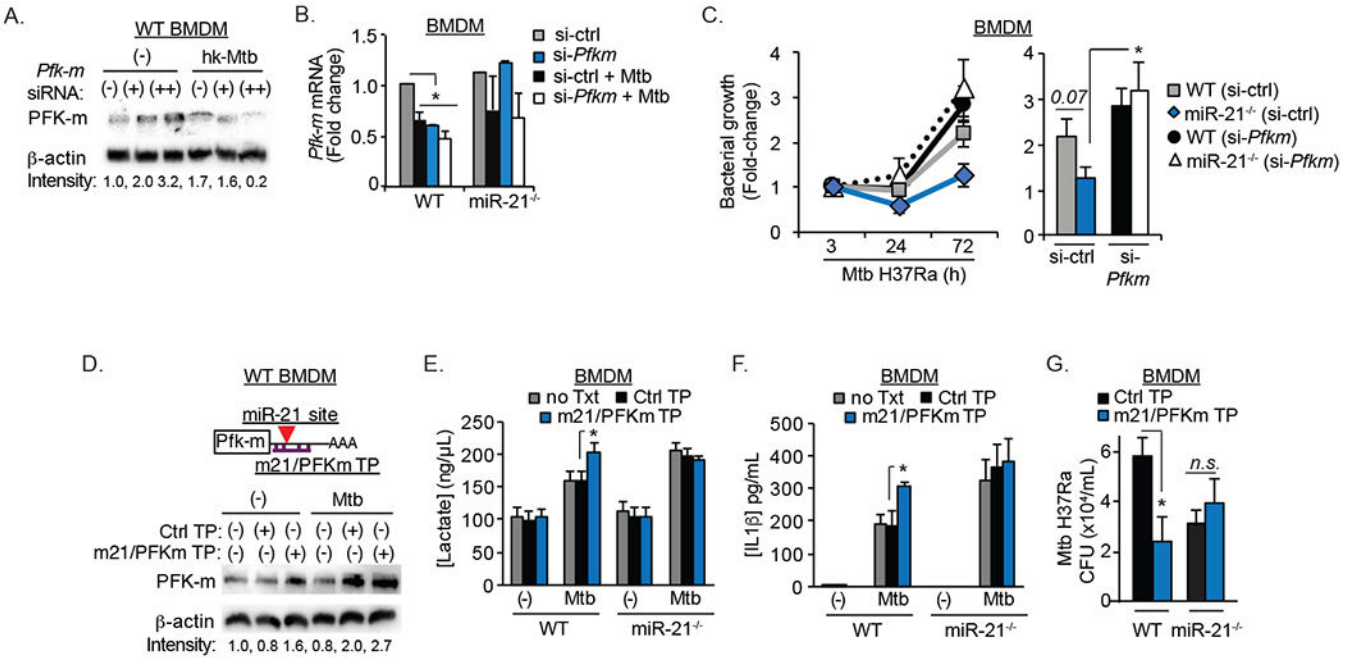

Figure 5.

Targeting of PFK-m by miR-21 controls Mtb responses. **A)** PFK-m mmunoblot in BMDM transfected with increasing amounts of *Pfk-m* specific siRNA (25 nM (+), 50 nM (++)) or control non-targeting siRNA (−), treated with hk-Mtb (MOI 5, 24h) alongside β-actin expression (loading control). **B)** qPCR of *Pfk-m* mRNA in BMDM (genotype indicated) transfected with 50 nM *Pfk-m* specific (si-*Pfk-m*) or control non-targeting (si-Ctrl) siRNA and subsequently infected with Mtb H37Ra (MOI 5, 24h). **C)** Bacterial growth in BMDM treated as B) upto 72h. **D)** Target protection schematic showing PFK-m 3'UTR and miR-21/PFK-m specific morpholino (m21/PFKm TP – top) and PFK-m immunoblot of BMDM transfected with 10 μM control non-targeting morpholino (Ctrl TP) or m21/PFK-m TP or empty transfected cells (−) and subsequently infected with Mtb H37Ra (MOI 5, 24h) or β-actin expression (loading control). **E-F)** Lactate production (E) or IL-1β ELISA (F) in supernatants from BMDM transfected with 10 μM non-targeting morpholino (Ctrl TP) or m21/PFKm TP or empty transfected cells (no Txt) and infected with Mtb H37Ra (Mtb, MOI 5, 24h). **G)** Bacterial CFUs of BMDM treated as in E) upto 72h. Blot is 1 experiment representative of n=2 (A) or n=3 independent experiments (D). mRNA data is fold-induction relative to uninfected si-Ctrl transfected WT BMDM (B). Bacterial growth is presented as fold-change in baseline CFU (3h) (C) or CFU values at 72h. Lactate and ELISA data is mean concentration (E-F). All data is mean ± sem of n=3 independent experiments. * $P < 0.05$, n.s. $P > 0.05$ for the indicated group comparisons (ANOVA with post-hoc Tukey tests).

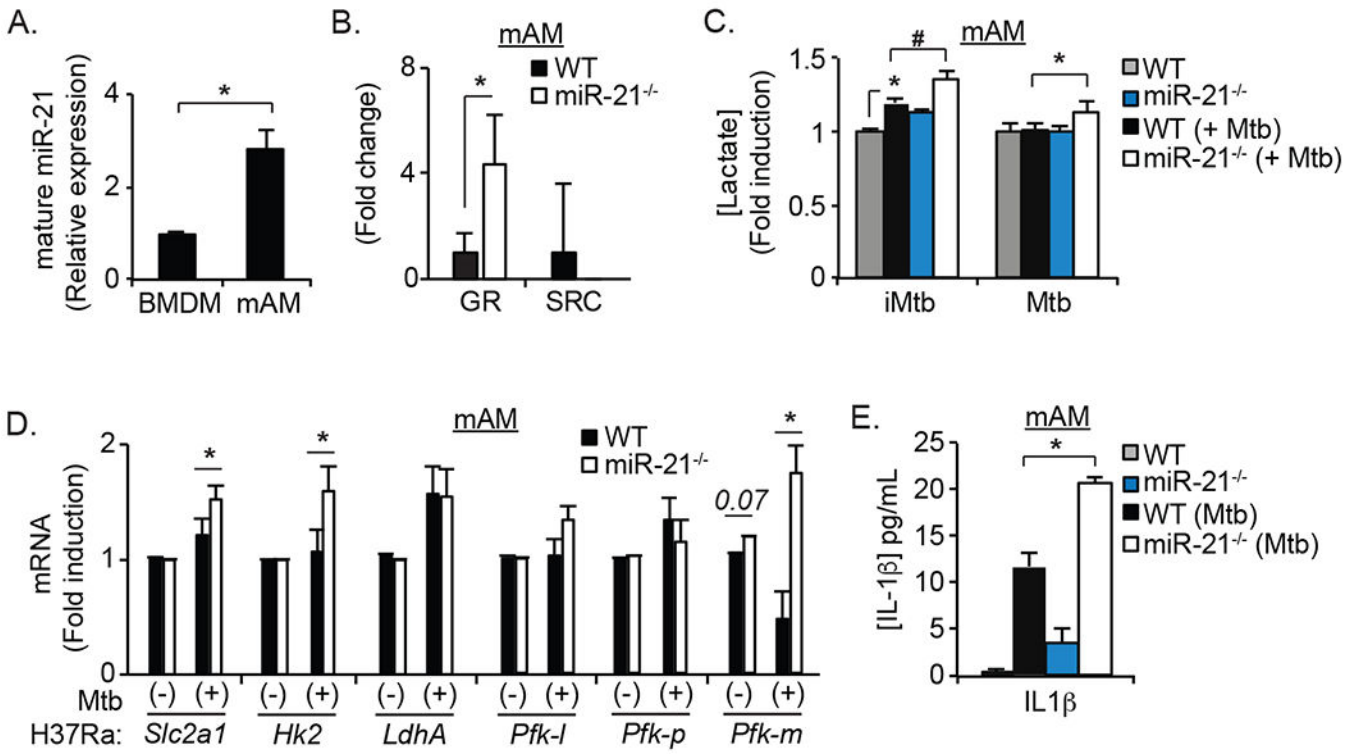

Figure 6.

miR-21 limits alveolar macrophage responses to Mtb infection. **A)** qPCR of mature miR-21 in resting BMDM or mouse alveolar macrophages (mAM). **B)** GR and SRC of resting BMDM or mAM (genotype indicated). **C)** Extracellular lactate from mAM (genotype indicated) treated with γ-irradiated Mtb (γMtb) or infected with Mtb H37Ra (Mtb, MOI 5, 24h). **D)** qPCR of indicated genes in mAM (genotype indicated) infected with Mtb H37Ra (MOI 5, 24h). **E)** IL-1β ELISA in supernatants from mAM treated as in D). Data in A) is normalized ΔCt values across cell types, B) is fold change in indicated parameter relative to WT mAM, C) is mean fold-change in Lactate production relative to uninfected WT mAM, D) is fold-induction relative to uninfected WT mAM and E) is mean concentration. All experiments are mean ± sem for n=3 mice per group. * and # $P < 0.05$ for the indicated group comparisons (ANOVA with post-hoc Tukey tests (C-E) or Student t-test (A-B).

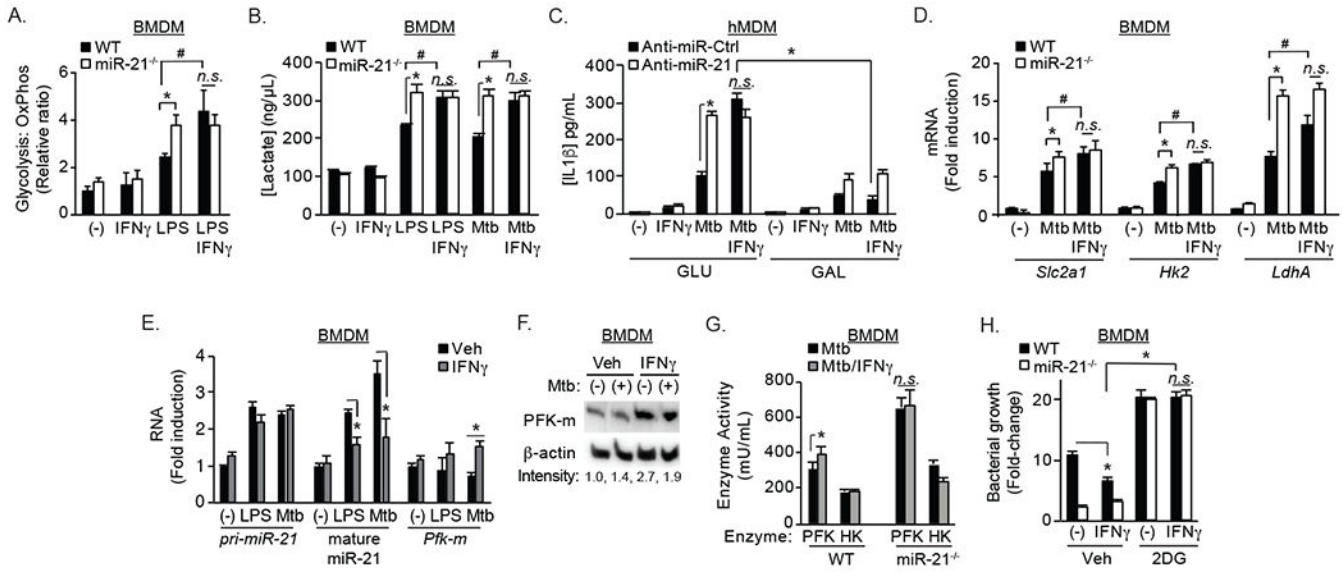

Figure 7.

Activation of macrophages by IFNγ targets glycolysis via miR-21. **A)** ECAR:OCR ratio in BMDM (genotype indicated) primed with IFNγ (5 ng/mL) before treatment with LPS (100 ng/mL). **B)** Extracellular lactate from BMDM (genotype indicated) primed with IFNγ (5 ng/mL) before treatment with LPS (100 ng/mL) or infection with Mtb H37Ra (MOI 5, 24h). **C)** IL-1β ELISA in supernatants from hMDM transfected with 50 nM miR-21-specific antisense (Anti-miR-21) or a control non-specific antisense (Anti-miR-Ctrl) 24h prior to treatment with IFNγ (5 ng/mL) and/or infection with Mtb H37Ra (MOI 5, 24h) in glucose-containing media (GLU) or glucose-free galactose-containing media (GAL). **D)** qPCR of indicated genes in BMDM (genotype indicated) primed with IFNγ (5 ng/mL) before infection with Mtb H37Ra (MOI 5, 24h). **E)** qPCR of indicated RNA species in BMDM primed with IFNγ (5 ng/mL) before treatment with LPS (100 ng/mL) or infection with Mtb H37Ra (MOI 5) for 24 h. **F)** PFK-m immunoblot of BMDM treated as in E). **G)** In-vitro enzyme activity for phosphofructokinase (PFK) or hexokinase (HK) in lysates from BMDM treated as in D. **H)** Bacterial growth in BMDM (genotype indicated) primed with IFNγ (5 ng/mL) before infection with Mtb H37Ra (MOI 5, 72h), with treatment with 10 mM 2DG or vehicle 3h post-infection. Data is mean fold-change over uninfected (A, D-E, H) or mean concentration (B-C, G). Data is mean ± sem of n=3 independent experiments (A-E, H), 1 blot representative of n=3 (F) or mean activity ± sem for n=6 (PFK) or n=5 (HK) independent experiments (G). * and # $P < 0.05$ for the indicated group comparisons (ANOVA with post-hoc Tukey tests).